Article

N^6-methyladenosine in poly(A) tails stabilize VSG transcripts

https://doi.org/10.1038/s41586-022-04544-0

Received: 18 December 2019

Accepted: 10 February 2022

Published online: 30 March 2022

Check for updates

Idálio J. Viegas[1], Juan Pereira de Macedo[1,8], Lúcia Serra[1,8], Mariana De Niz[1], Adriana Temporão[1], Sara Silva Pereira[1], Aashiq H. Mirza[2], Ed Bergstrom[3,4], João A. Rodrigues[1,5], Francisco Aresta-Branco[1,6,7], Samie R. Jaffrey[2] & Luisa M. Figueiredo[1]✉

RNA modifications are important regulators of gene expression[1]. In *Trypanosoma brucei*, transcription is polycistronic and thus most regulation happens post-transcriptionally[2]. N^6-methyladenosine (m^6A) has been detected in this parasite, but its function remains unknown[3]. Here we found that m^6A is enriched in 342 transcripts using RNA immunoprecipitation, with an enrichment in transcripts encoding variant surface glycoproteins (VSGs). Approximately 50% of the m^6A is located in the poly(A) tail of the actively expressed VSG transcripts. m^6A residues are removed from the VSG poly(A) tail before deadenylation and mRNA degradation. Computational analysis revealed an association between m^6A in the poly(A) tail and a 16-mer motif in the 3′ untranslated region of VSG genes. Using genetic tools, we show that the 16-mer motif acts as a *cis*-acting motif that is required for inclusion of m^6A in the poly(A) tail. Removal of this motif from the 3′ untranslated region of VSG genes results in poly(A) tails lacking m^6A, rapid deadenylation and mRNA degradation. To our knowledge, this is the first identification of an RNA modification in the poly(A) tail of any eukaryote, uncovering a post-transcriptional mechanism of gene regulation.

Trypanosoma brucei is a protozoan unicellular parasite that causes lethal diseases in sub-Saharan Africa: sleeping sickness in humans and nagana in cattle[4]. The infection can last several months or years, mostly because *T. brucei* escapes the immune system by periodically changing its VSG[2]. The *T. brucei* genome contains around 2,000 antigenically distinct VSG genes[5], but only one VSG gene is actively transcribed at a given time. Transcriptionally silent VSG genes are switched on by homologous recombination into the bloodstream expression site (BES) or by transcriptional activation of a new BES[2], resulting in parasites covered by approximately 10 million identical copies of the VSG protein[6].

VSG is essential for the survival of bloodstream form (BSF) parasites. VSG is not only one of the most abundant proteins in *T. brucei* but it is also the most abundant mRNA in BSFs (4–11% of total mRNA)[7,8]. VSG mRNA abundance is a consequence of its unusual transcription by RNA polymerase I and its prolonged stability[9]. The half-life of VSG mRNA has been estimated to range from 90 to 270 min, contrasting with the 12 min, on average, for other transcripts[10]. The basis for its unusually high stability is not known. It is thought to derive from the 3′ untranslated region (UTR) of VSG genes, which contains two conserved motifs, a 9-mer and a 16-mer motif (usually called 16-mer, but the first and last positions are less conserved; the conserved core is a 14-mer), found immediately upstream of the poly(A) tail[5,11]. Mutational studies have shown that the 16-mer motif is essential for the high abundance and stability of VSG mRNAs[12], even though its underlying mechanism is unknown.

VSG expression is highly regulated when the BSF parasites undergo differentiation to the procyclic forms (PCFs) that proliferate in the insect vector[13]. The BES becomes transcriptionally silenced and VSG mRNA becomes unstable[14], which results in rapid loss of VSG mRNA and replacement of the VSG coat protein by other surface proteins (reviewed in ref. [15]). The mechanism by which VSG mRNA becomes unstable during differentiation remains unknown. The surface changes are accompanied by additional metabolic and morphological adaptations, which allow PCFs to survive in a different environment in the insect host[15].

RNA modifications have recently been identified as important means of regulating gene expression. The most abundant internal modified nucleotide in eukaryotic mRNA is N^6-methyladenosine (m^6A)[16,17], which is widespread across the human and mouse transcriptomes and is often found near stop codons and the 3′ UTR of the mRNA encoded by multiple genes[18,19]. m^6A is synthesized by a methyltransferase complex whose catalytic subunit, METTL3, methylates adenosine in a specific consensus motif. Demethylases responsible for removing m^6A from mRNA have also been identified[20,21]. m^6A affects several aspects of RNA biology, for instance, contributing to mRNA stability, mRNA translation or affecting alternative polyadenylation site selection (reviewed in ref. [1]).

Here we show that m^6A is an RNA modification enriched in *T. brucei* mRNA. This study revealed that m^6A is present in the poly(A) tails of mRNA, and approximately half of m^6A is located in only one transcript (VSG mRNA). We identified a *cis*-acting element that is required for inclusion of m^6A at the VSG poly(A) tail and, by genetically manipulating this motif, we showed that m^6A blocks poly(A) deadenylation, hence promoting the stability of VSG mRNA. We provide evidence that the poly(A) tails of mRNA can be methylated in eukaryotes, and that they have a regulatory role in the control of gene expression.

[1]Instituto de Medicina Molecular—João Lobo Antunes, Faculdade de Medicina, Universidade de Lisboa, Lisbon, Portugal. [2]Department of Pharmacology, Weill Medical College, Cornell University, New York, NY, USA. [3]Department of Chemistry, University of York, York, UK. [4]Centre of Excellence in Mass Spectrometry, University of York, York, UK. [5]Present address: Clarify Analytical, Évora, Portugal. [6]Division of Immune Diversity, German Cancer Research Center, Heidelberg, Germany. [7]Division of Structural Biology of Infection and Immunity, German Cancer Research Center, Heidelberg, Germany. [8]These authors contributed equally: Juan Pereira de Macedo, Lúcia Serra. ✉e-mail: lmf@medicina.ulisboa.pt

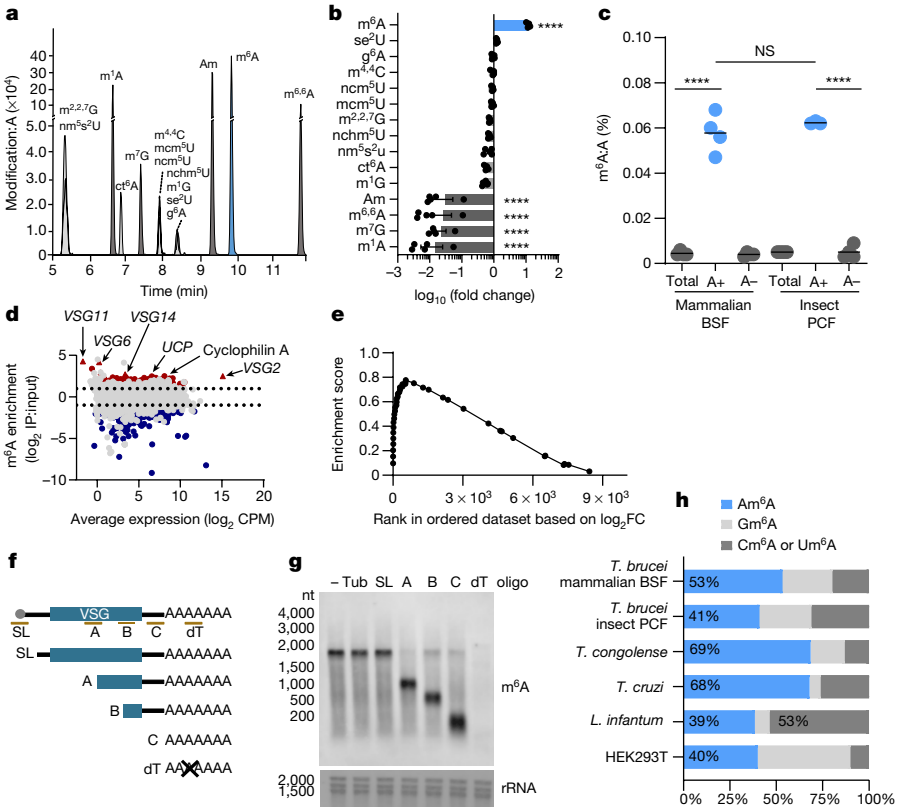

Fig. 1 | m⁶A is present in the poly(A) tail of VSG mRNA and other transcripts. **a**, Overlap chromatogram of nucleoside modifications detected in mRNA mammalian BSFs by liquid chromatography–tandem mass spectrometry. Data are ratios between peak areas. For definitions of compounds, see Extended Data Fig. 1. **b**, Enrichment of nucleoside modifications in mRNA relative to total RNA. Two-way analysis of variance (ANOVA) with Sidak correction for multiple test (Am, m⁶A, m⁶,⁶A, m⁷G and m¹A, ****$P < 0.0001$). $n = 5$ biological samples. **c**, Levels of m⁶A quantified using standard curve in Extended Data Fig. 2d. The bar represents the mean. $n = 3$ or 4 biological replicates. Unpaired two-tailed *t*-test: mammalian bloodstream or insect total RNA versus mRNA $P < 0.0001$; mammalian bloodstream mRNA versus insect procyclic mRNA $P = 0.4162$. NS, not significant. **d**, Scatter plot of m⁶A enrichment relative to average transcript expression, expressed as $\log_2$ counts per million reads mapped (CPM). Transcripts enriched or depleted in the m⁶A IP sample relative to the input sample are indicated in red or blue, respectively. Moderated *t*-test adjusted with Benjamin–Hochberg false discovery rate. For *P* values, see Supplementary Table 1. Dotted lines, values of 1 and −1 in the *y* axis ($\log_2$ IP:input), which were used for statistical analysis. Triangles represent VSG genes. $n = 3$ independent IPs. **e**, Gene set enrichment analysis. The line indicates the enrichment score distribution across VSG genes, ranked according to the $\log_2$ fold change ($\log_2$FC) between m⁶A IP and input samples. **f**, Schematics of oligonucleotides used in RNase H digestion of VSG mRNA and expected digestion products (**g**). dT, poly deoxi-thymidines; SL, spliced leader. **g**, m⁶A immunoblotting of mammalian BSF total RNA digested with RNase H after pre-incubation with indicated oligonucleotides (oligo). Methylene blue stains rRNA. Tub, β-tubulin. $n = 2$ independent experiments. **h**, Mass spectrometry analysis of total RNA digested independently with enzymes RNase T1 and RNase A. Total RNA was extracted from *T. brucei* (BSF, $n = 3$; PCF, $n = 2$), *T. congolense* ($n = 2$), *T. cruzi* ($n = 1$), *L. infantum* ($n = 2$) and human cells (HEK293T, $n = 1$) (Supplementary Fig. 1, Source Data Fig. 1).

m⁶A is enriched in the VSG poly(A) tail

To investigate whether *T. brucei* RNA has modified nucleosides that could have a role in gene regulation, we used liquid chromatography–tandem mass spectrometry to detect possible modifications of RNA nucleosides in poly(A)-enriched RNA (mRNA) and total RNA (mainly composed of rRNA, tRNA and other non-coding RNAs). Thirty-four modified nucleosides were detected: 15 were detected in mRNA and 19 were only detected in total RNA (Fig. 1a, Extended Data Fig. 1, Extended Data Table 1). Some of these modifications had been previously detected in *T. brucei* RNA including Am, which is found in the mRNA cap structure, and m³C, m⁵C and Gm in tRNA and rRNA[22–24]. Comparison of the intensities of each RNA nucleoside in mRNA versus total RNA revealed that m⁶A is tenfold more abundant in mRNA. Ten other modifications are equally distributed in mRNA and total RNA and four modifications are 30–60-fold more enriched in total RNA than in mRNA (Fig. 1b). Given the importance of m⁶A for RNA metabolism in other eukaryotes, we focused on this specific modification in *T. brucei*.

We used an m⁶A nucleoside standard to quantify m⁶A in poly(A)-enriched, poly(A)-depleted and total RNA fractions from two stages of the parasite life cycle, that is, the mammalian BSF and the insect PCF. The chromatograms of the poly(A)-enriched fraction (mRNA) revealed a peak corresponding to 282→150 mass transition and an elution time of 10 min (Extended Data Fig. 2a), identical to the elution time observed in the m⁶A standard. The m⁶A peak was barely detectable in the total and poly(A)-depleted RNA, indicating that most (if not all) m⁶A is present in mRNA and absent from rRNA and tRNAs. Similar results were obtained in RNA fractions from the PCF insect stage (Extended Data Fig. 2b). For both stages of the life cycle, the chromatograms of total RNA and poly(A)-depleted samples contained a peak with an identical mass transition, but an earlier elution time (6.5 min), which probably reflects m¹A (Extended Data Fig. 2c), a modification that is commonly found in rRNAs and tRNAs[25,26].

The m⁶A standard allowed us to quantify the abundance of m⁶A in mRNA fractions of BSFs and PCFs (Extended Data Fig. 2d): m⁶A represents 0.06–0.14% of total adenines in mRNA (Fig. 1c, Extended Data Fig. 2e). In other words, in 10,000 adenosines, 6–14 are methylated to form m⁶A. This proportion is lower than in mammalian cells (0.1–0.4%[16,17]).

To identify the transcripts enriched in m⁶A, we performed m⁶A RNA immunoprecipitation (m⁶A-RIP) in non-fragmented RNA, followed by

sequencing of both input and immunoprecipitated (IP) transcripts. Similar strategies have been described before to study methylation at the gene level[27,28]. Differential expression analysis showed that *VSG2* is the most represented transcript in the IP sample. To calculate the enrichment of m^{6}A per transcript, we normalized the number of reads in the IP sample by the number of reads in the input sample. Figure 1d shows that *VSG2* is the transcript with highest average expression ($\log_2$ counts per million reads mapped = 15.1; *x* axis) and one of the most enriched in m^{6}A ($\log_2$ fold change = 2.5; *y* axis). Seven of the top ten genes are VSG or VSG-related. Gene set enrichment analysis showed that VSG transcripts are indeed enriched in m^{6}A (Fig. 1e). Non-VSG transcripts can also be enriched in m^{6}A, such as those encoding cyclophilin A and ubiquitin carrier protein (UCP) (Fig. 1d).

To confirm that VSG is the transcript with the most m^{6}A and to map m^{6}A within the VSG transcript, we performed immunoblotting with an antibody that specifically recognizes m^{6}A (Extended Data Fig. 3a) and in which we site-selectively cleaved the VSG transcript with ribonuclease H (RNase H). Total RNA was incubated with DNA oligonucleotides that annealed at different sites along the length of the VSG transcript. RNase H digestion of the RNA–DNA hybrids result in fragments of predicted sizes (Fig. 1f). If the VSG transcript is the band with the intense m^{6}A signal, the band detected by immunoblotting would 'shift' to one or more fragments of smaller size.

In the control condition, in which RNA was pre-incubated without any oligonucleotide or with a control oligonucleotide that annealed with β-tubulin (another abundant transcript in *T. brucei*), we observed an m^{6}A-positive smear, confirming that m^{6}A is present in multiple mRNA molecules. However, we also observed an intense band of around 1.8 kb, which coincides with the size of actively transcribed VSG (Fig. 1g, Extended Data Fig. 3b). This prominent band corresponds to 50% of the m^{6}A signal; it is not detected in mRNA from the insect stage of the parasite life cycle (in which VSG is not expressed), nor in mouse liver RNA (Extended Data Fig. 3c, d). A band of similar mobility was also observed when we used an oligonucleotide that hybridized to the spliced leader (SL) sequence, a 39-nucleotide (nt) sequence that contains the mRNA cap and that is added to every mRNA by a *trans*-splicing reaction[29]. This indicates that m^{6}A is neither present in the spliced leader sequence, nor in the mRNA cap structure. By contrast, when we used oligonucleotides VSG-A, VSG-B and VSG-C, which hybridized to three different unique sites in the VSG sequence, we observed that the major m^{6}A band shifted, and in all three conditions, the 3′-end fragment contained the entire m^{6}A signal (Fig. 1g). The VSG-C oligonucleotide is adjacent to the beginning of the poly(A) tail. Thus, the 3′ fragment released upon RNase H digestion with VSG-C corresponds to the poly(A) tail of VSG mRNA. This fragment, which contains the entire m^{6}A signal from the VSG transcript, is heterogeneous in length and shorter than 200 nt (Fig. 1g).

To further confirm that the 3′ fragment released after incubation with VSG-C and RNase H corresponded to the VSG poly(A) tail, we performed RNase H digestion in RNA pre-incubated with a poly(T) oligonucleotide. Consistent with the results using VSG-C, the major band detected by the m^{6}A antibody completely disappears, further supporting the idea that in BSFs, most m^{6}A is present in the poly(A) tail of VSG mRNA (Fig. 1f, g). Digestion of RNA hybridized with poly(T) also abolished the smear detected by the m^{6}A antibody (Fig. 1g), indicating that most m^{6}A present in non-VSG transcripts appears to be located in their poly(A) tails. Of note, a similar approach to digest poly(A) tails does not affect the levels of m^{6}A in mammalian mRNA of mouse[18].

Most m^{6}A in mRNA from human cells is preceded by guanosine[30,31]. As m^{6}A in *T. brucei* appears to be localized in the poly(A) tail, we wanted to understand whether m^{6}A is in a similar sequence context in trypanosome mRNA. To test this, we performed RNA digestion with selective nucleases, similar to assays originally performed to establish the m^{6}A sequence context in mammals[30]. In these experiments, we digested trypanosome RNA with RNase T1, which cleaves RNA after G, or RNase A, which cleaves RNA after pyrimidines (C/U). These enzymes leave the subsequent nucleotide with a 5′-hydroxyl. Thus, if m^{6}A follows G or C/U, it would be released with a 5′-hydroxyl, after RNase T1 or RNase A digestion, respectively. Next, the RNA is digested with nuclease P1, which leaves any other m^{6}A with a 5′-phosphate. m^{6}A can then be quantified using isotope-labelled m^{6}A as a standard. m^{6}A that is preceded by an A can be extrapolated by subtracting total m^{6}A levels from m^{6}A preceded by G and C/U. Using this approach, m^{6}A in mammalian mRNA is primarily preceded by G (Fig. 1h), as previously described[30]. However, m^{6}A in *T. brucei* BSF mRNA was primarily preceded by A (53%), and only 27% of m^{6}A was preceded by G (Fig. 1h). This is consistent with a strong enrichment of m^{6}A in the poly(A) tails. We also tested m^{6}A in related species: *Trypanosoma congolense*, *Trypanosoma cruzi* and *Leishmania infantum*. *Trypanosoma congolense* and *T. cruzi* showed an even higher enrichment of m^{6}A after an A (69% and 68%, respectively) (Fig. 1h). By contrast, *L. infantum* showed a unique digestion pattern, in which 53% of m^{6}A was located after a C or a U (Fig. 1h). With these results, we predict that the three more closely related species, *T. brucei*, *T. congolense* and *T. cruzi*, have a large fraction of m^{6}A in the poly(A) tail of transcripts, whereas *L. infantum* contains m^{6}A in an internal region of the transcripts and in a consensus motif different from mammalian cells.

Our results show that trypanosomatids have a large fraction of m^{6}A in a sequence context different from mammalian cells. In *T. brucei*, although transcripts from more than 300 genes have m^{6}A, the VSG gene family is the most represented. We have also shown that around 50% of m^{6}A in a cell is present in the poly(A) tail of the actively transcribed VSG mRNA. On the basis of the m^{6}A frequency in the *T. brucei* transcriptome and the enrichment in VSG genes, we estimate that there are nearly four m^{6}A molecules per VSG mRNA.

Timing of m^{6}A removal

The half-life of VSG transcripts is 90–270 min, whereas the median mRNA half-life in trypanosomes is 13 min (ref. [10]). Given that removal of the poly(A) tail often precedes RNA degradation, we hypothesized that the presence of m^{6}A in the poly(A) tail could contribute to this exceptional stability in VSG mRNA.

We tracked the levels of m^{6}A in VSG mRNA as it undergoes degradation in three independent conditions. We first inhibited transcription in BSF parasites with actinomycin D and, for the next 6 h, we quantified the amount of VSG mRNA that remained by quantitative PCR with reverse transcription (RT–qPCR). We also measured the levels of m^{6}A in VSG genes (by immunoblotting) and the length of the VSG poly(A) tail using northern blotting and the poly(A) tail length assay, which involves ligation of adaptors to the 3′ end of poly(A) tails and two consecutive PCRs using VSG-specific forward primers (Fig. 2a). The amplified fragments contain part of the open reading frame, the 3′ UTR of VSG transcripts and the downstream poly(A) tail, whose size is variable between different transcript molecules.

VSG mRNA has previously been shown to exhibit biphasic decay: in the first hour after transcription blocking, the levels of VSG remain high and, only in a second phase, do the levels of VSG mRNA decay exponentially[14,32]. Consistent with these earlier findings, we detected no major changes in mRNA abundance during the first hour after treatment with actinomycin D (lag phase or first phase); however, afterwards, VSG genes exhibited exponential decay (second phase) (Fig. 2b). Northern blotting and the poly(A) tail-length assay revealed that during the 1-h lag phase, the length of the VSG poly(A) tail was stable, but then it rapidly shortened during the second phase (Fig. 2c, Extended Data Fig. 4). At 120 min and 240 min, the intensity of the VSG poly(A) tail dropped rapidly, indicating that the transcript was also rapidly degraded. This indicates that there is a specific time-dependent step that triggers the rapid shortening of the VSG poly(A) tail and the subsequent degradation of the VSG transcript. Immunoblotting revealed that the levels of m^{6}A also decreased, but, notably, the loss of m^{6}A preceded the shortening of the poly(A) tail and subsequent mRNA decay (Fig. 2b, d, Extended

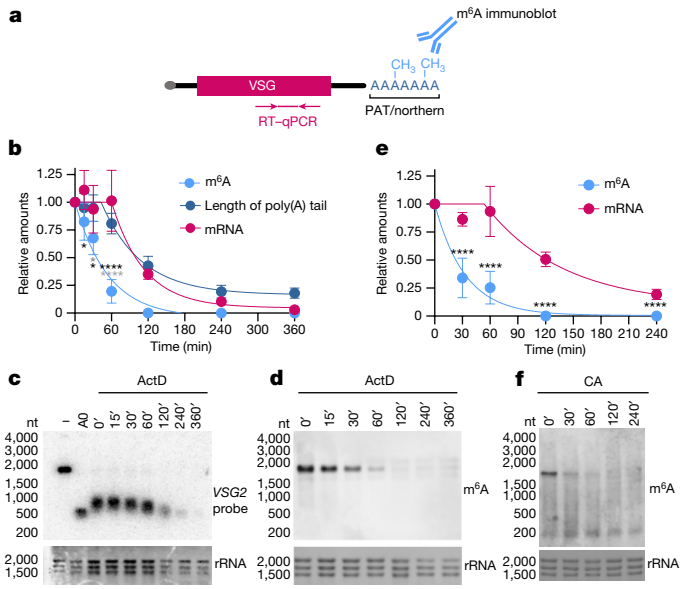

Fig. 2 | m^{6}A is removed from VSG mRNA before its degradation. **a**, Schematics of VSG mRNA transcripts and analyses described in this figure. **b**, VSG transcript levels (RT–qPCR, pink), m^{6}A levels (immunoblotting, light blue) and the length of the poly(A) tail (poly(A) tailing (PAT) assay, dark blue) after transcription was halted by actinomycin D (ActD). Data are mean ± s.d. Two-way ANOVA with Sidak correction for multiple test. The black asterisks denote significance between mRNA and m^{6}A. The grey asterisks denote significance between poly(A) tail and m^{6}A (****P < 0.0001, *P = 0.0104 in mRNA versus m^{6}A in 15 min, *P = 0.0224 in mRNA versus m^{6}A in 30 min, *P = 0.0169 in poly(A) versus m^{6}A in 30 min). n = 3 transcription inhibition experiments. **c**, Northern blotting of VSG decay from parasites treated with ActD. Total RNA was incubated with an oligonucleotide located 368 nt upstream of the VSG poly(A) tail and digested with RNaseH. The probe hybridizes with the conserved 16-mer motif. A0 is the VSG 3′-end fragment in which the poly(A) tail was removed by oligo dT-RNase H digestion. Methylene blue stains rRNA. n = 3 transcription inhibition experiments. Quantification is shown in Extended Data Fig. 4. **d**, m^{6}A immunoblotting of BSF total RNA extracted from parasites treated with ActD (**c**). Methylene blue stains rRNA. Quantification is shown in Extended Data Fig. 4. **e**, VSG transcript levels and m^{6}A levels during parasite differentiation from BSF to PCF. Total RNA was extracted at different time points after inducing differentiation with *cis*-aconitate (CA). The same colour code as in **b**. Data are mean ± s.d. Two-way ANOVA with Sidak correction for multiple test (****P < 0.0001). n = 3 parasite differentiation experiments. **f**, m^{6}A immunoblotting of parasites differentiating to PCFs (**e**). Methylene blue stains rRNA (Supplementary Fig. 1, Source Data Fig. 2).

Data Fig. 4). In fact, the levels of m^{6}A decrease exponentially during the first hour after treatment with actinomycin D, taking around 35 min for total mRNA m^{6}A levels to drop by 50%, whereas VSG mRNA only reached half of the steady-state levels around 2 h (Fig. 2b). These results indicate that m^{6}A is removed from VSG mRNA before the deadenylation of the poly(A) tail, which is quickly and immediately followed by degradation of the transcript.

When BSF parasites undergo cellular differentiation to PCFs, VSG genes are downregulated as a consequence of decreased transcription and decreased mRNA stability[14]. To test whether m^{6}A is also rapidly removed from VSG mRNA before its developmentally programmed degradation, we induced differentiation in vitro by adding *cis*-aconitate to the medium and changing the temperature to 27 °C. Parasites were collected and total RNA was extracted in different time points. RT–qPCR showed that the levels of VSG mRNA stayed stable for around 1 h, which was followed by an exponential decay (Fig. 2e). Immunoblotting analysis showed that during parasite differentiation, m^{6}A intensity in the VSG mRNA dropped faster than the levels of VSG mRNA, reaching half of the steady-state levels in 23 min (Fig. 2e, f). Thus, during parasite differentiation, we observed again that the removal of m^{6}A precedes the loss of VSG mRNA levels.

Overall, these results show that in two independent conditions, m^{6}A is removed from the VSG transcript earlier than the VSG transcript is deadenylated and degraded, suggesting that m^{6}A may need to be removed from the VSG transcript before it can be degraded.

VSG mRNA is methylated in the nucleus

In most organisms, m^{6}A is generated by methylation of adenosine residues within a specific consensus sequence by the METTL3 methyltransferase or its orthologues[1]. Given that in *T. brucei* m^{6}A is present in the poly(A) tail, a different mechanism is probably used. Indeed, trypanosomes lack a METTL3 orthologue[33], indicating that a different pathway would be required to acquire m^{6}A in the poly(A) tail. To understand how m^{6}A accumulates in the VSG mRNA, we used parasite differentiation as a natural inducible system of VSG gene downregulation. This process is reversible in the first 2 h (ref. [34]). Parasite differentiation was induced by adding *cis*-aconitate for 30 min (as described above; Fig. 2e), and then was washed away (Fig. 3a). Immunoblotting revealed that m^{6}A intensity of the VSG band was reduced after 30 min of treatment with *cis*-aconitate (Fig. 3b, c), whereas mRNA levels remained unchanged (Fig. 3d). When cells were allowed to recover for 1 h in the absence of *cis*-aconitate (flask 4, Fig. 3a), we observed that the intensity of the m^{6}A signal returned to normal levels (Fig. 3c), whereas mRNA levels continued to remain constant (Fig. 3d). These results indicate that the levels of m^{6}A can be recovered without a net increase in VSG mRNA levels. The net levels of VSG mRNA result from a balance between de novo transcription and degradation. To test whether the recovery of m^{6}A levels after the removal of *cis*-aconitate was due to de novo transcription, parasites were cultured in the presence of actinomycin D (flask 5, Fig. 3a). We observed that the intensity of m^{6}A in the VSG transcripts was not recovered. Instead, the levels of m^{6}A decreased to approximately 20% (Fig. 3c). Overall, these results indicate that de novo transcription is required to re-establish m^{6}A levels in VSG mRNA.

If m^{6}A is incorporated into VSG mRNA soon after transcription, and if it remains in the poly(A) tail until it gets degraded, we should be able to detect m^{6}A in the nucleus and in the cytoplasm of the parasites. Immunofluorescence analysis with an antibody to m^{6}A showed a punctate pattern in both the nucleus (20%) and the cytoplasm (80%) (Fig. 3e, f, Extended Data Fig. 5a). To confirm that this m^{6}A signal originated from RNA, we incubated the fixed cells with nuclease P1, which specifically cleaves single-stranded nucleic acids without any sequence-specific requirement, before the antibody staining. This treatment caused a marked reduction in the intensity of the m^{6}A signal, indicating that the immunoreactivity of the m^{6}A antibody derives from RNA, and not from non-specific interactions with cellular proteins (Fig. 3e, g, Extended Data Fig. 5b). As an additional control, we treated the cells with actinomycin D for 2 h before immunofluorescence analysis. This treatment is expected to result in reduced levels of cellular mRNA. Immunostaining with the m^{6}A antibody showed a drop in the intensity of the m^{6}A signal by around 40% (Fig. 3e, g, Extended Data Fig. 5b), which is similar to the trend observed by immunoblotting (Fig. 2c). Overall, these data show that the m^{6}A immunostaining probably reflects m^{6}A in mRNA and validates the immunoblotting results.

To understand how m^{6}A is incorporated into VSG mRNA, we performed RNA-FISH analysis of *VSG2* (Fig. 3h) and compared it with m^{6}A localization (Fig. 3e). Quantification of the FISH signal revealed that approximately 19% of the signal is in the nucleus and 81% is in the cytoplasm (Fig. 3i, Extended Data Fig. 5c). Given that this transcript distribution is very similar to the subcellular distribution of m^{6}A, the data suggest that the concentration of m^{6}A per transcript is relatively similar in the two compartments. To confirm this hypothesis, we biochemically fractionated parasites into nuclear and cytoplasmic fractions and quantified m^{6}A in each fraction. Fractionation was confirmed by DAPI

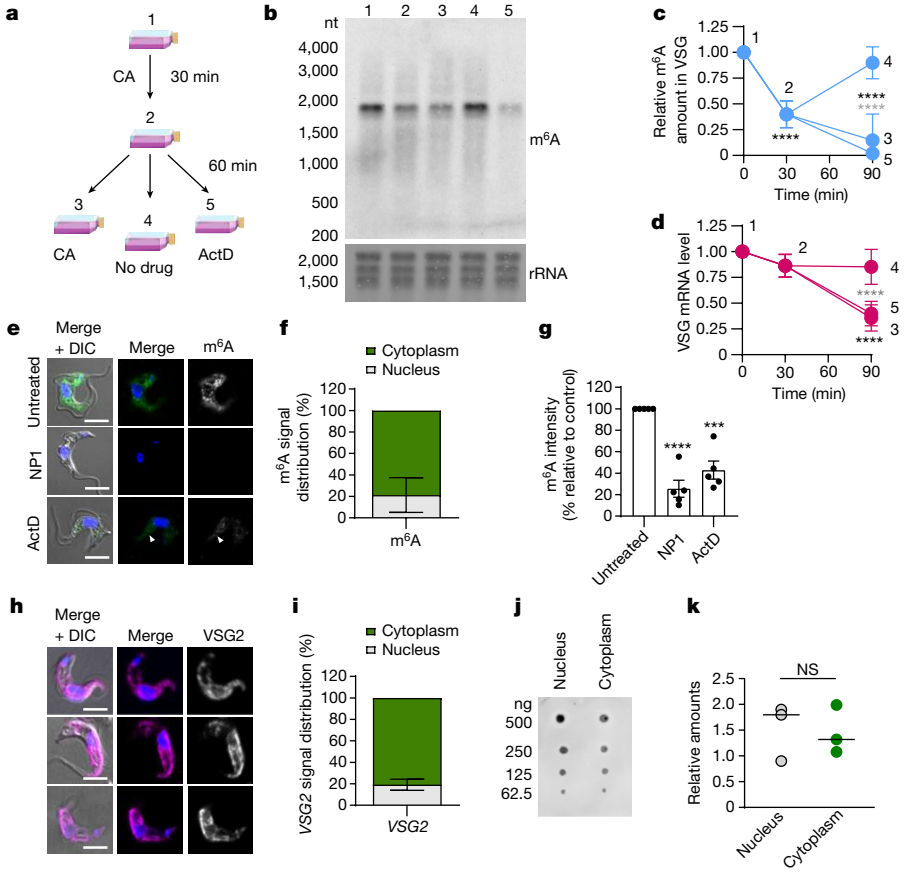

Fig. 3 | Inclusion of m^{6}A in the VSG poly(A) tail depends on de novo transcription. a, Parasites were treated with CA, and after washing away the compound, parasites were placed in culture in three different conditions. Labels 1–5 indicate the conditions at which parasites were collected for immunoblotting analysis (**b**). Drawings were obtained from smart.servier.com. **b**, m^{6}A immunoblot at each of the five conditions (**a**). $n = 3$ independent experiments. **c**, Quantification of immunoblotting in **a**. Two-way ANOVA with Sidak correction for multiple test (****$P < 0.0001$). Data are mean ± s.d. The black asterisks refer to condition 3. The grey asterisks refer to condition 5. **d**, VSG mRNA levels measured by RT–qPCR. Two-way ANOVA with Sidak correction for multiple test (****$P < 0.0001$). Data are mean ± s.d. $n = 3$ independent experiments. **e**, m^{6}A immunofluorescence analysis. Parasites were treated with nuclease P1 (NP1) or ActD. Nuclei were stained with Hoechst. The white arrowheads point to a weak m^{6}A signal. Scale bars, 4 µm. DIC, differential interference contrast. **f**, Proportion of m^{6}A signal in the nucleus and cytoplasm from immunofluorescence analysis. $n = 4$ experiments with 125 parasites in each. Data are mean ± s.d. **g**, Levels of m^{6}A expressed as mean fluorescence intensity (MFI). Unpaired two-tailed *t*-test (****$P < 0.0001$, ***$P = 0.001$). Data are mean ± s.e.m. $n = 5$ independent experiments. **h**, RNA-FISH analysis of *VSG2* transcripts. Three representative cells are shown. Scale bars, 4 µm. **i**, Proportion of the *VSG2* mRNA signal in the nucleus and cytoplasm from FISH analysis. (**h**). Data are mean ± s.d. $n = 5$ independent experiments with 34 parasites in each. **j**, m^{6}A dot-blot of subcellular fractions. The quantity of spotted RNA is indicated. $n = 3$ fractionation experiments. **k**, Quantification of the dot-blot m^{6}A signal (**j**). Unpaired two-tailed *t*-test ($P = 0.8753$). Data are median (Supplementary Fig. 1, Source Data Fig. 3).

staining of the nuclei and western blotting (Extended Data Fig. 5d, e). Equal masses of RNA from nuclear and cytoplasmic fractions were spotted on a nylon membrane and hybridized with anti-m^{6}A antibody (Fig. 3j). Quantification of the m^{6}A signal showed that the intensity of m^{6}A was similar in the two fractions (Fig. 3k), revealing that the concentration of m^{6}A per transcript is similar in the two cell compartments.

Together, our data indicate that methylation of the poly(A) tail of VSG mRNA takes place in the nucleus, soon after transcription.

A VSG motif is required for methylation

m^{6}A is added to the VSG mRNA poly(A) tail soon after transcription, probably still in the nucleus. The m^{6}A-RIP analysis showed that m^{6}A is particularly enriched in VSG transcripts (Fig. 2d). We therefore asked how the VSG poly(A) tails are selected for preferential enrichment of m^{6}A. It has previously been shown that each VSG gene contains a conserved 16-mer motif (5′-TGATATATTTTAACAC-3′) in the 3′ UTR adjacent to the poly(A) tail that is necessary for the stability of VSG mRNA[12]. It has been recently shown that an RNA-binding complex binds to this motif and stabilizes the transcript by a yet unknown mechanism[12,35]. Here we hypothesized that this 16-mer motif may act in *cis* to promote inclusion of m^{6}A of the adjacent poly(A) tail.

VSGs are essential proteins that are transcribed monoallelically from a telomeric location called the BES. If we mutagenized the 16-mer motif from the monoallelically transcribed *VSG2* gene, this would reduce the levels of the VSG2 protein, which is lethal for the parasites[12]. To solve this problem, a *VSG2*-expressing parasite line was genetically modified to introduce a reporter VSG gene (*VSG117*) in the same BES by homologous recombination. The resulting cell lines were called VSG double expressors (DEs), because they simultaneously express the endogenous *VSG2* and the reporter *VSG117* (Fig. 4a). In the DE1 cell line, the *VSG117* gene contained a wild-type 16-mer motif (16-mer^{WT}). In the DE2 cell line, *VSG117* contained a 16-mer motif in which the sequence was scrambled (5′-GTTATACAAAACTTTT-3′) (Fig. 4a). As has previously been reported, the transcript levels of *VSG2* and *VSG117* are dependent on each other and are dependent on the presence of the 16-mer motif[12]. RT–qPCR analysis showed that the two VSG genes have roughly the same levels in the DE1 cell line. However, in the DE2 cell line, the *VSG117* transcript is about sevenfold less abundant than the *VSG2* transcript (Fig. 4b), confirming that the 16-mer motif is important for the abundance of VSG transcripts.

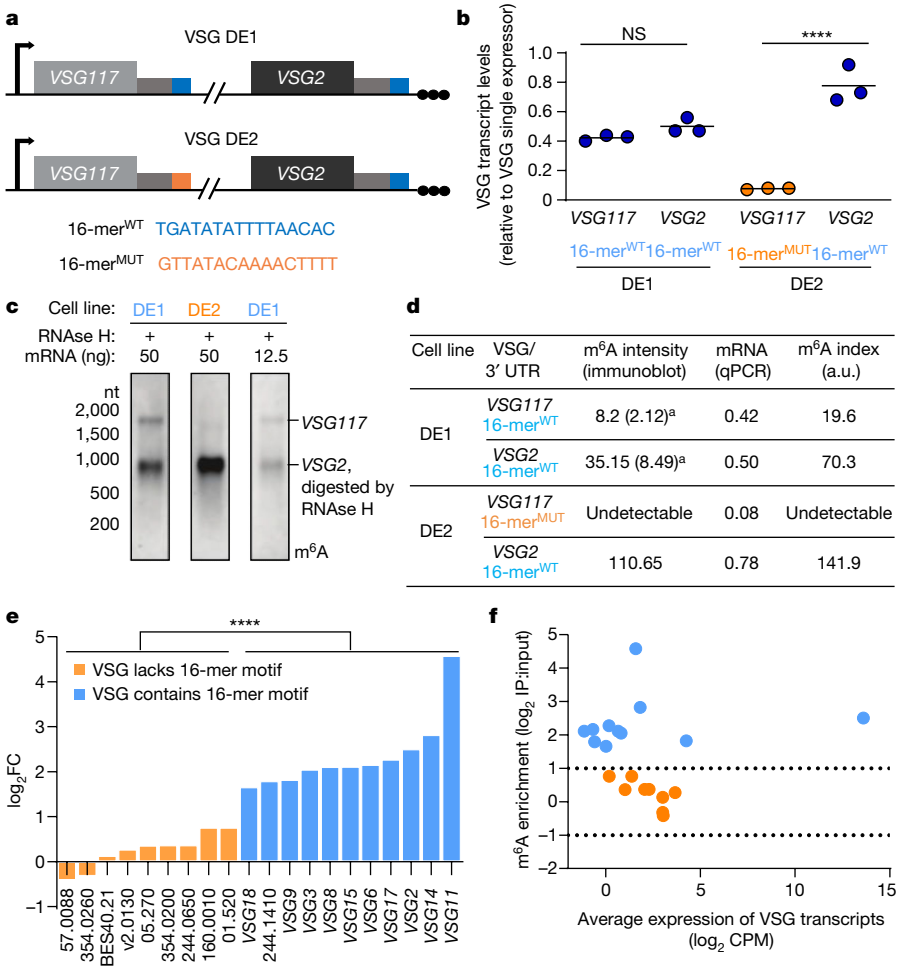

Cell line	VSG/ 3′ UTR	m^{6}A intensity (immunoblot)	mRNA (qPCR)	m^{6}A index (a.u.)
DE1	*VSG117* 16-mer^{WT}	8.2 (2.12)[a]	0.42	19.6
	VSG2 16-mer^{WT}	35.15 (8.49)[a]	0.50	70.3
DE2	*VSG117* 16-mer^{MUT}	Undetectable	0.08	Undetectable
	VSG2 16-mer^{WT}	110.65	0.78	141.9

Fig. 4 | Conserved VSG 16-mer motif is required for inclusion of m^{6}A in an adjacent poly(A) tail. a, Schematics of VSG DE cell lines. *VSG117* was inserted in the active BES, which contains *VSG2* at the telomeric end. In DE1, *VSG117* contains its endogenous 3′ UTR with the conserved 16-mer motif (sequence in blue). In DE2, the 16-mer motif of *VSG117* was scrambled (sequence in orange). **b**, Transcript levels of *VSG117* and *VSG2* transcripts (RT–qPCR), normalized to transcript levels in cell lines expressing only *VSG2*. One-way ANOVA with Sidak correction for multiple test ($P = 0.7612$ for *VSG2* WT versus *VSG117* WT in DE1, $^{****}P < 0.0001$ for *VSG2* WT versus *VSG117* MUT in DE2). $n = 3$ independent clones. Bars denote the mean. **c**, m^{6}A immunoblot of mRNA from DE1 and DE2 cell lines. RNase H digestion of *VSG2* mRNA was used to resolve *VSG2* and *VSG117* transcripts. Of DE1, 50 ng and 12.5 ng were loaded in two separate lanes. $n = 3$ independent clones. **d**, The m^{6}A index calculated as the ratio of m^{6}A intensity and mRNA levels, measured in **c** and **b**, respectively. [a]Intensities measured in lane 3 in **c**. **e**, m^{6}A enrichment in VSG genes. m^{6}A RIP sequencing data were used to calculate, for each VSG gene, the ratio between the number of aligned reads in IP versus input samples. Only VSG transcripts detected in the IP sample were used for this analysis. The blue and orange bars indicate the presence or absence, respectively, of the 16-mer motif in the 3′ UTR. Unpaired two-sided Mann–Whitney test ($^{****}P < 0.0001$). **f**, Scatter plot of m^{6}A RIP enrichment relative to transcript levels of detectable VSG transcripts. The colour code is identical to **e**. The dotted lines represent $\log_2$FC = 1 and $\log_2$FC = −1. Spearman correlation between the data was $R = -0.35$. $n = 3$ for input samples and m^{6}A IP samples (Supplementary Fig. 1, Source Data Fig. 4).

To test whether the 16-mer motif is required for inclusion of m^{6}A in VSG poly(A) tails, we performed m^{6}A immunoblotting of cellular RNA obtained from the two DE cell lines. Given that *VSG2* and *VSG117* transcripts have similar sizes (approximately 1.8 kb), we used RNase H to selectively cleave *VSG2* before resolving the RNA on gel. Cleavage of *VSG2* was performed by incubating the poly(A) RNA sample with an oligonucleotide that hybridizes to the open reading frame of *VSG2* followed by incubation with RNase H (as described in Fig. 1f, g). As expected, the fragment containing *VSG2* m^{6}A is smaller and runs faster on an agarose gel (Fig. 4c). An 'm^{6}A index' was calculated by dividing the relative intensity of m^{6}A in each VSG band (Fig. 4c) by the corresponding relative transcript levels measured by RT–qPCR (Fig. 4b). A low m^{6}A index indicates that a given transcript has fewer modified nucleotides (Fig. 4d).

Whenever the 3′ UTR of VSG transcripts contained a 16-mer^{WT} (VSG genes with a blue box in Fig. 4a), VSG m^{6}A bands were detectable by immunoblot and the m^{6}A index varied between 20 and 140 arbitrary units. By contrast, when the 16-mer motif was mutagenized (16-mer^{MUT}; *VSG117* with an orange box in Fig. 4a), the VSG m^{6}A was undetectable (Fig. 4c), and the m^{6}A index therefore was too low to calculate. These results indicate that the motif is required for inclusion of m^{6}A in the VSG transcript. If the 16-mer motif had no role in m^{6}A inclusion, the *VSG117* m^{6}A index would be identical in both cell lines (DE1 and DE2), that is, around 20. Given that the RT–qPCR quantifications showed that the relative intensity of *VSG117* 16-mer^{MUT} is approximately 0.10 (Fig. 4b), the predicted intensity of the *VSG117* 16-mer^{MUT} m^{6}A band would have been $20 \times 0.10 = 2.0$ arbitrary units. To be sure that a band with this level of m^{6}A would be detected on an immunoblot, we ran a more diluted DE1 RNA sample in lane 3 (Fig. 4c). The intensity of the *VSG117* 16-mer^{WT} band is 2.1 arbitrary units (Fig. 4c, d), and it was readily detected in the immunoblot. Given that we could not detect any band corresponding to a putative methylated *VSG117* 16-mer^{MUT} in DE2 (even after over exposure of the immunoblot, Extended Data Fig. 6a), we conclude that the VSG-conserved 16-mer motif is necessary for the inclusion

of m^{6}A in the VSG poly(A) tail. A similar immunoblotting analysis was performed in an independent pair of DE cell lines (DE3 and DE4) that express a different reporter VSG (*VSG8*) (Extended Data Fig. 6b, c). Consistently, m^{6}A was not detectable when the 16-mer motif of *VSG8* was mutagenized, further supporting the conclusion that this motif is required for detectable methylation.

To determine whether the 16-mer motif is associated with the presence of m^{6}A in the VSG transcript, we used the m^{6}A-RIP data to compare the enrichment of m^{6}A in VSG transcripts with and without a 16-mer motif (Fig. 4e). m^{6}A enrichment is calculated as the ratio between the number of normalized reads in IP samples versus input samples. Among the 20 VSG transcripts detected after IP (Fig. 1d), we found that the 11 VSG transcripts with a 16-mer motif (blue bars) are, on average, fivefold more enriched in m^{6}A than the nine VSG transcripts lacking a 16-mer motif (orange bars) ($\log_2$ fold change = 2.1, $P < 0.0001$, Mann–Whitney test) (Fig. 4e). The 11 transcripts with a 16-mer motif encode fully functional VSG proteins or one pseudogene and all genes are located in the specialized subtelomeric loci from where VSG can be transcribed (BES). By contrast, the nine VSG transcripts that lack the 16-mer motif are located in non-BES sites and most of them (seven) are pseudogenes.

To confirm that the enrichment of m^{6}A detected in VSG genes containing a 16-mer motif was not simply a reflection of higher expression of those VSG genes, the transcript levels measured from the m^{6}A-RIP input sample were plotted against m^{6}A enrichment for each of the 20 detected VSG genes (Fig. 4f). As expected, *VSG2* is the active gene and with the largest counts per million reads mapped. We found no correlation between m^{6}A enrichment and transcript levels, indicating that the yield of m^{6}A enrichment in the IP experiment is not dependent on the abundance of the transcript. This data indicate that the observation that the transcripts containing the 16-mer motif are more enriched in m^{6}A is independent of VSG transcript levels and reflects the functional link between the 3′ UTR motif and the presence of m^{6}A in the adjacent poly(A) tail.

m^{6}A is required for VSG mRNA stability

The unusual localization of m^{6}A in the poly(A) tail suggests that the underlying biochemistry of m^{6}A formation in trypanosomes is different from what has been described in other eukaryotes. Consistently, sequence searches using hidden Markov models (http://hmmer.org/) did not find a METTL3 methyltransferase, nor Alkbh5 demethylase orthologues in kinetoplastida[33]. Given that at this stage the mechanism of m^{6}A formation in the poly(A) tail is unknown and therefore cannot be directly blocked, we used the genetic mutants of the 16-mer conserved motif to enquire about the function of m^{6}A in VSG mRNA.

To test the role of the 16-mer motif on poly(A) length in mRNA stability, we measured VSG mRNA stability in the 16-mer^{WT} and 16-mer^{MUT} cell lines. The half-life of VSG mRNA was measured by blocking transcription for 1 h with actinomycin D (the duration of the lag phase during decay of VSG mRNA) and the levels of VSG mRNA were followed by RT–qPCR. The poly(A) tail-length assay clearly shows that, when the *VSG117* transcript contains the 16-mer motif (16-mer^{WT} cell line), the length of the *VSG117* poly(A) tail is stable for 1 h (Fig. 5a, b). By contrast, *VSG117* transcripts containing a scrambled 16-mer motif exhibited very rapid shortening of the poly(A) tail. In this case, there was no detectable lag phase—instead, the length of the poly(A) tail was reduced to 25% of its original length after just 15 min, and was undetectable after 1 h (Fig. 5a, b). Consistent with the fast kinetics of poly(A) deadenylation, in the absence of an intact 16-mer motif, the transcript levels of *VSG117* decayed very rapidly with a half-life of approximately 20 min (Fig. 5b). These experiments show that when the VSG conserved 16-mer motif is mutated and m^{6}A is lost, the VSG transcript is no longer stable and exhibits rapid poly(A) deadenylation and a marked reduction of mRNA stability.

CAF1 is the deadenylase responsible for the deadenylation of most transcripts in *T. brucei*[36]. Here we asked whether CAF1 also deadenylates VSG mRNA and whether the presence of m^{6}A affected this process. To test this, we downregulated *CAF1* by tetracycline-inducible RNA interference (Extended Data Fig. 7). We followed the decay of the *VSG2* transcript and its poly(A) tail length after treatment with actinomycin D (Fig. 5c, d). In WT conditions (−Tet condition), the shortening of the poly(A) tail and the decrease in the transcript levels of VSG started 1 h post-treatment with actinomycin D and the poly(A) tail was entirely deadenylated in 4 h (Fig. 5c, d). By contrast, when *CAF1* was downregulated, in the first 2 h after treatment with actinomycin D, both the length of the poly(A) tail and the transcript levels of VSG remained unchanged. Only after 4 h, we saw a slightly shorter poly(A) tail and a decrease in the transcript levels of VSG.

The fact that the phenotype of CAF1 depletion is only detected after 1 h post-treatment with actinomycin D demonstrates that CAF1 does not have strong activity on the VSG poly(A) tail during the first hour of treatment. Given our previous finding that it takes about 1 h to remove m^{6}A from VSG mRNA (Fig. 2b), CAF1 may be partially inhibited while the VSG poly(A) tail is methylated, but once m^{6}A has been removed from the poly(A) tail, CAF1 may then be able to rapidly deadenylate the VSG transcript.

To further understand the mechanism by which m^{6}A inhibits deadenylation of VSG, we performed RNA-FISH to determine the subcellular localization of VSG. Given that CAF1 is localized predominantly in the cytoplasm[37], we predicted that a VSG transcript with a mutagenized 16-mer motif (and hence lower levels of m^{6}A) would be unaffected in the nucleus, but would be rapidly degraded by CAF1 in the cytoplasm. To test this, we genetically modified the CAF1-inducible RNA interference cell line to have a reporter VSG (*VSG8*) where the 16-mer motif was either WT or mutagenized (Fig. 5e, f, Extended Data Fig. 6b).

When *VSG8* had a WT 16-mer motif, depletion of CAF1 led to a small increase in the abundance of the *VSG8* transcript and *VSG8* remained distributed at approximately 20% in the nucleus and 80% in cytoplasm relative to the condition when CAF1 was present (Fig. 5e, f). By contrast, when the 16-mer motif of *VSG8* was mutagenized (that is, when m^{6}A levels are undetectable) and CAF1 was present, the levels of *VSG8* in the cytoplasm showed a sharp decrease, whereas the nuclear signal was less affected (Fig. 5e, f). Finally, when the 16-mer motif was mutagenized and CAF1 was depleted, we observed a significant recovery of the *VSG8* RNA-FISH signal, especially in the cytoplasm, indicating that CAF1 is responsible for deadenylating most mutagenized VSG transcripts and that this process takes place in the cytoplasm (Fig. 5e, f).

In the two conditions in which *VSG8* had 16-mer^{MUT}, the nuclear levels of *VSG8* were substantially lower (the mean fluorescence intensity is around 100) than in the conditions where *VSG8* had 16-mer^{WT} (the mean fluorescence intensity is around 200) (Fig. 5e, f). These results suggest that when the levels of m^{6}A are reduced in the poly(A) tail, the stability of the VSG mRNA is also partially reduced in the nucleus and this appears to be independent of CAF1.

Together, these data are consistent with a model in which m^{6}A inhibits the activity of CAF1 in the cytoplasm, reducing poly(A) deadenylation and thus contributing to VSG mRNA stability.

Discussion

The classic function of a poly(A) tail is to suppress mRNA degradation and to promote translation. Poly(A)-binding proteins bind to the poly(A) tail and stimulate mRNA translation by interaction with translation initiation factors[38]. Removal of the poly(A) tail by deadenylase complexes is a prerequisite for mRNAs to enter into 5′ to 3′ or 3′ to 5′degradation pathways[39,40]. In this Article, we identified a mechanism by which a poly(A) tail contributes to mRNA stability. We found that the presence of m^{6}A in the poly(A) tail of VSG transcripts inhibits RNA degradation, most probably by impeding CAF1-mediated deadenylation.

The presence of m^{6}A in the poly(A) tail is so far unique to trypanosomes. In other eukaryotes, m^{6}A has mainly been detected by m^{6}A mapping approaches around the stop codon and the 3′ UTR, where it has a

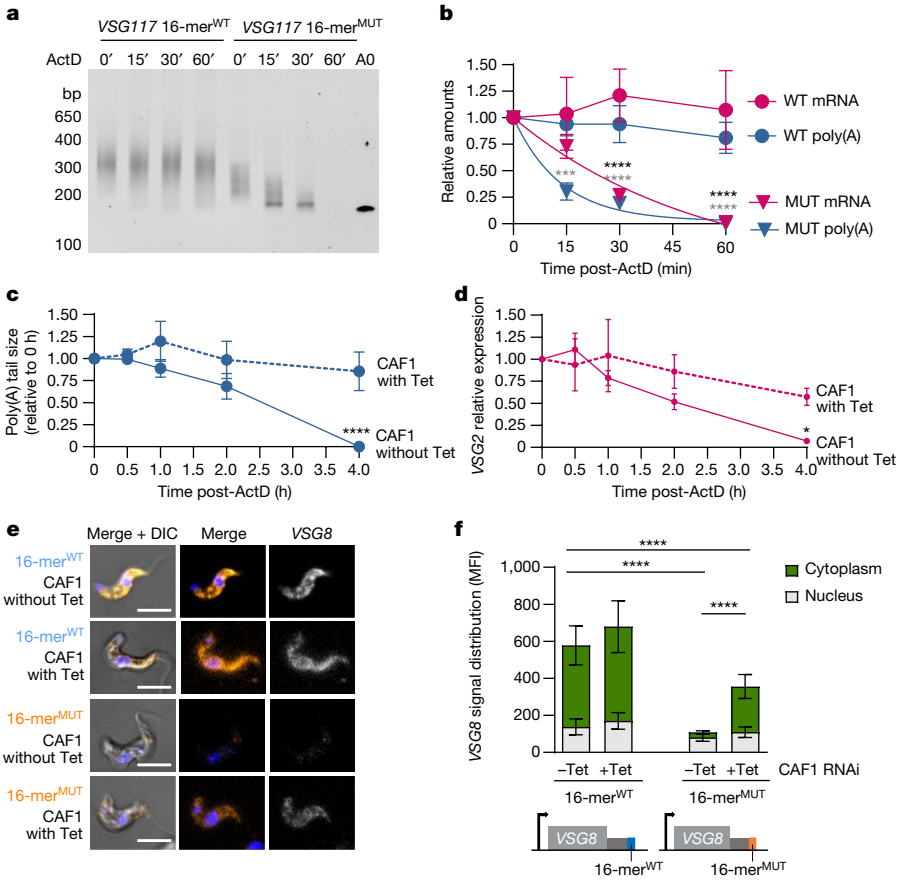

Fig. 5 | VSG 16-mer motif inhibits CAF1 and poly(A) tail deadenylation. **a**, The length of the VSG poly(A) tail was measured using the PAT assay after transcription was halted by ActD. 16-mer^{WT} and 16-mer^{MUT} cell lines were compared. **b**, *VSG117* transcript levels (measured by RT–qPCR, pink) and the length of the poly(A) tail (measured by PAT assay, blue) after transcription was halted by ActD. Values were normalized to 0 h. Two-way ANOVA with Sidak correction for multiple test. The black asterisks refer to mRNA. The grey asterisks refer to the poly(A) tail (****$P < 0.0001$, ***$P = 0.0002$ in *VSG117* WT poly(A) tail versus *VSG117* MUT poly(A) tail in 15 min). Data are mean ± s.d. $n = 3$ transcription inhibition experiments. **c**, Length of the VSG poly(A) tail upon CAF1 downregulation and after transcription was halted by ActD. The length of the poly(A) was measured by the PAT assay. Two-way ANOVA with Sidak correction for multiple test (****$P < 0.0001$). Data are mean ± s.d. $n = 3$ transcription inhibition experiments. Tet, tetracycline. **d**, VSG transcript levels upon CAF1 downregulation and after transcription was halted by ActD. Significance was measured by two-way ANOVA with Sidak correction for multiple test (*$P = 0.0191$). Data are mean ± s.d. $n = 3$ transcription inhibition experiments. **e**, RNA-FISH analysis of *VSG8* of four indicated conditions. Scale bars, 4 µm. **f**, *VSG8* transcript levels expressed as MFI levels of the FISH signal. The proportion of nuclear and cytoplasmic staining was calculated as described in Fig. 3. Data are mean ± s.d. Unpaired two-sided *t*-test (****$P < 0.0001$). $n = 4$ biological replicates, 100 cells per replicate (Supplementary Fig. 1, Source Data Fig. 5). RNAi, RNA interference.

role in mRNA stability and translation[1]. A mapping study was recently published in *T. brucei* in which m^{6}A was mapped in internal regions of transcripts[3]. m^{6}A was not reported to be in the poly(A) tail in this previous study. However, m^{6}A mapping relies on aligning m^{6}A-containing RNA fragments to the genomic sequence. As the poly(A) sequence is not encoded in the genome, any m^{6}A-containing poly(A) tail would not be mappable and therefore not detected in this or any other previous m^{6}A mapping study.

It remains unclear how m^{6}A gets into the poly(A) tail. The presence of m^{6}A in the poly(A) tail suggests that an unusual RNA methyltransferase directly or indirectly binds to the 16-mer motif and methylates adenosines that are either adjacent to the 16-mer motif or become more proximal via a loop-like conformation of the poly(A) tail. This would explain why orthologues of the canonical METTL3 enzyme do not exist in the trypanosome genome[33]. A recent study has shown that a RNA-stabilizing complex, the MKT1 complex, binds to the 16-mer motif[35], but this complex does not contain any homologues of m^{6}A readers, writers or erasers.

Deadenylation is the first step in the main mRNA decay pathway in eukaryotes[41]. *Trypanosoma brucei* is not an exception[29]. In this study, we showed that m^{6}A seems to protect the poly(A) tail from deadenylation by CAF1. The molecular mechanism behind this stabilizing effect is unknown. It is possible that the CAF1 deadenylase is inefficient on a methylated poly(A) tail. There is structural and biochemical evidence that poly(A) tails adopt a tertiary structure that facilitates recognition by some mammalian deadenylases (CAF1 and Pan2)[42]. When a poly(A) tail contains m^{6}A, the tertiary structure may not be properly formed and deadenylase activity is inhibited, as has been shown with guanosine residues within an oligo-A oligonucleotide[42]. In this model, a putative demethylase may be required to remove the methyl group, which could then allow the VSG poly(A) tail to be efficiently deadenylated by CAF1. Alternatively, the stabilizing effect of m^{6}A could result from the recruitment of a specific RNA-binding protein, that prevents the poly(A) tail from being deadenylated.

Trypanosoma brucei has around 2,000 VSG genes, but only one is actively transcribed at a given time[2]. The Rudenko laboratory has proposed that the maximal amount of VSG mRNA per cell is dependent on a post-transcriptional limiting factor that is determined by the presence of the 16-mer motif[12]. The inclusion of m^{6}A in poly(A) tails may be this factor. When the 16-mer motif is present in both VSG genes, both get partially methylated and their abundance is reduced to about half

of a single VSG expressor; however, when the 16-mer motif is absent from one of the VSG genes, the second VSG is more methylated and the transcripts become more abundant.

To our knowledge, our work is the first report of an RNA modification in poly(A) tails. We show that m^{6}A is present in the poly(A) tail of *T. brucei* mRNAs, it is enriched in the most abundant transcript (VSG), and that m^{6}A acts as a protecting factor stabilizing VSG transcripts from CAF1 deadenylation activity. It will be important for future studies to identify the enzymes and proteins involved in adding, reading or removing m^{6}A. Given the importance of VSG regulation for chronic infection and parasite transmission, drugs that interfere with m^{6}A incorporation in poly(A) tails are expected to block parasite virulence. Understanding these regulatory epitranscriptomic processes may open up possibilities for developing therapeutic strategies to treat sleeping sickness.

Online content

Any methods, additional references, Nature Research reporting summaries, source data, extended data, supplementary information, acknowledgements, peer review information; details of author contributions and competing interests; and statements of data and code availability are available at https://doi.org/10.1038/s41586-022-04544-0.

1. Zaccara, S., Ries, R. J. & Jaffrey, S. R. Reading, writing and erasing mRNA methylation. *Nat. Rev. Mol. Cell Biol.* **20**, 608–624 (2019).
2. Horn, D. Antigenic variation in African trypanosomes. *Mol. Biochem. Parasitol.* **195**, 123–129 (2014).
3. Liu, L. et al. Differential m^{6}A methylomes between two major life stages allows potential regulations in *Trypanosoma brucei*. *Biochem. Biophys. Res. Commun.* **508**, 1286–1290 (2019).
4. Franco, J. R., Simarro, P. P., Diarra, A., Ruiz-Postigo, J. A. & Jannin, J. G. The journey towards elimination of gambiense human African trypanosomiasis: not far, nor easy. *Parasitology* **141**, 748–760 (2014).
5. Cross, G. A., Kim, H. S. & Wickstead, B. Capturing the variant surface glycoprotein repertoire (the VSGnome) of *Trypanosoma brucei* Lister 427. *Mol. Biochem. Parasitol.* **195**, 59–73 (2014).
6. Cross, G. A. Identification, purification and properties of clone-specific glycoprotein antigens constituting the surface coat of *Trypanosoma brucei*. *Parasitology* **71**, 393–417 (1975).
7. Nilsson, D. et al. Spliced leader trapping reveals widespread alternative splicing patterns in the highly dynamic transcriptome of *Trypanosoma brucei*. *PLoS Pathog.* **6**, e1001037 (2010).
8. Kraus, A. J., Brink, B. G. & Siegel, T. N. Efficient and specific oligo-based depletion of rRNA. *Sci Rep.* **9**, 12281 (2019).
9. Gunzl, A. et al. RNA polymerase I transcribes procyclin genes and variant surface glycoprotein gene expression sites in *Trypanosoma brucei*. *Eukaryot. Cell* **2**, 542–551 (2003).
10. Fadda, A. et al. Transcriptome-wide analysis of trypanosome mRNA decay reveals complex degradation kinetics and suggests a role for co-transcriptional degradation in determining mRNA levels. *Mol. Microbiol.* **94**, 307–326 (2014).
11. Berberof, M. et al. The 3′-terminal region of the mRNAs for VSG and procyclin can confer stage specificity to gene expression in *Trypanosoma brucei*. *EMBO J.* **14**, 2925–2934 (1995).
12. Ridewood, S. et al. The role of genomic location and flanking 3′UTR in the generation of functional levels of variant surface glycoprotein in *Trypanosoma brucei*. *Mol. Microbiol.* **106**, 614–634 (2017).
13. Roditi, I. et al. Procyclin gene expression and loss of the variant surface glycoprotein during differentiation of *Trypanosoma brucei*. *J. Cell Biol.* **108**, 737–746 (1989).
14. Ehlers, B., Czichos, J. & Overath, P. RNA turnover in *Trypanosoma brucei*. *Mol. Cell. Biol.* **7**, 1242–1249 (1987).
15. Matthews, K. R. The developmental cell biology of *Trypanosoma brucei*. *J. Cell Sci.* **118**, 283–290 (2005).
16. Wei, C. M., Gershowitz, A. & Moss, B. Methylated nucleotides block 5′ terminus of HeLa cell messenger RNA. *Cell* **4**, 379–386 (1975).
17. Perry, R. P., Kelley, D. E., Friderici, K. & Rottman, F. The methylated constituents of L cell messenger RNA: evidence for an unusual cluster at the 5′ terminus. *Cell* **4**, 387–394 (1975).
18. Meyer, K. D. et al. Comprehensive analysis of mRNA methylation reveals enrichment in 3′ UTRs and near stop codons. *Cell* **149**, 1635–1646 (2012).
19. Dominissini, D. et al. Topology of the human and mouse m^{6}A RNA methylomes revealed by m^{6}A-seq. *Nature* **485**, 201–206 (2012).
20. Jia, G. et al. N^6-methyladenosine in nuclear RNA is a major substrate of the obesity-associated FTO. *Nat. Chem. Biol.* **7**, 885–887 (2011).
21. Zheng, G. et al. ALKBH5 is a mammalian RNA demethylase that impacts RNA metabolism and mouse fertility. *Mol. Cell* **49**, 18–29 (2013).
22. Freistadt, M. S., Cross, G. A. & Robertson, H. D. Discontinuously synthesized mRNA from *Trypanosoma brucei* contains the highly methylated 5′ cap structure, m^{7}GpppA*A*C(2′-O)mU*A. *J. Biol. Chem.* **263**, 15071–15075 (1988).
23. Bangs, J. D., Crain, P. F., Hashizume, T., McCloskey, J. A. & Boothroyd, J. C. Mass spectrometry of mRNA cap 4 from trypanosomatids reveals two novel nucleosides. *J. Biol. Chem.* **267**, 9805–9815 (1992).
24. Perry, K. L., Watkins, K. P. & Agabian, N. Trypanosome mRNAs have unusual "cap 4" structures acquired by addition of a spliced leader. *Proc. Natl Acad. Sci. USA* **84**, 8190–8194 (1987).
25. Hauenschild, R. et al. The reverse transcription signature of *N*-1-methyladenosine in RNA-seq is sequence dependent. *Nucleic Acids Res.* **43**, 9950–9964 (2015).
26. Boccaletto, P. et al. MODOMICS: a database of RNA modification pathways. 2017 update. *Nucleic Acids Res.* **46**, D303–D307 (2018).
27. Molinie, B. et al. m^{6}A-LAIC-seq reveals the census and complexity of the m^{6}A epitranscriptome. *Nat. Methods* **13**, 692–698 (2016).
28. Xiang, J. F. et al. N^6-methyladenosines modulate A-to-I RNA editing. *Mol. Cell* **69**, 126–135. e6 (2018).
29. Clayton, C. E. Regulation of gene expression in trypanosomatids: living with polycistronic transcription. *Open Biol.* **9**, 190072 (2019).
30. Schibler, U., Kelley, D. E. & Perry, R. P. Comparison of methylated sequences in messenger RNA and heterogeneous nuclear RNA from mouse L cells. *J. Mol. Biol.* **115**, 695–714 (1977).
31. Linder, B. et al. Single-nucleotide-resolution mapping of m^{6}A and m^{6}Am throughout the transcriptome. *Nat. Methods* **12**, 767–772 (2015).
32. Hoek, M., Zanders, T. & Cross, G. A. M. *Trypanosoma brucei* expression-site-associated-gene 8 protein interacts with a *Pumilio* family protein. *Mol. Biochem. Parasitol.* **120**, 269–283 (2002).
33. Iyer, L. M., Zhang, D. & Aravind, L. Adenine methylation in eukaryotes: apprehending the complex evolutionary history and functional potential of an epigenetic modification. *Bioessays* **38**, 27–40 (2016).
34. Domingo-Sananes, M. R., Szoor, B., Ferguson, M. A., Urbaniak, M. D. & Matthews, K. R. Molecular control of irreversible bistability during trypanosome developmental commitment. *J. Cell Biol.* **211**, 455–468 (2015).
35. Melo do Nascimento, L. et al. Functional insights from a surface antigen mRNA-bound proteome. *eLife* **10**, e68136 (2021).
36. Fadda, A., Färber, V., Droll, D. & Clayton, C. The roles of 3′-exoribonucleases and the exosome in trypanosome mRNA degradation. *RNA* **19**, 937–947 (2013).
37. Schwede, A. et al. A role for Caf1 in mRNA deadenylation and decay in trypanosomes and human cells. *Nucleic Acids Res.* **36**, 3374–3388 (2008).
38. Gallie, D. R. The role of the poly(A) binding protein in the assembly of the Cap-binding complex during translation initiation in plants. *Translation (Austin)* **2**, e959378 (2014).
39. Garneau, N. L., Wilusz, J. & Wilusz, C. J. The highways and byways of mRNA decay. *Nat. Rev. Mol. Cell Biol.* **8**, 113–126 (2007).
40. Chen, C. Y. & Shyu, A. B. Mechanisms of deadenylation-dependent decay. *Wiley Interdiscip. Rev. RNA* **2**, 167–183 (2011).
41. Decker, C. J. & Parker, R. A turnover pathway for both stable and unstable mRNAs in yeast: evidence for a requirement for deadenylation. *Genes Dev.* **7**, 1632–1643 (1993).
42. Tang, T. T. L., Stowell, J. A. W., Hill, C. H. & Passmore, L. A. The intrinsic structure of poly(A) RNA determines the specificity of Pan2 and Caf1 deadenylases. *Nat. Struct. Mol. Biol.* **26**, 433–442 (2019).

Reporting summary

Further information on research design is available in the Nature Research Reporting Summary linked to this paper.

Data availability

RNA sequencing datasets of m^{6}A-RIP experiments are deposited in the Sequence Read Archive under the accession code: PRJNA786734. The following panels have associated raw figures: 1b, c, e, h, 2b, c, 3c, d, f, g, i, k, 4b, e, f, 5b–d, f, Extended Data Figs. 2d, e, 3c, 4, 5a–c, 7. The following public databases were used; Trypanosome genome database (TryTrypDB): https://tritrypdb.org/tritrypdb/app; and RNA modifications database (MODOMICS): http://genesilico.pl/modomics/. All data are available on request from the corresponding author. Source data are provided with this paper.

Acknowledgements We are grateful to support from the Howard Hughes Medical Institute International Early Career Scientist Program (55007419), a European Molecular Biology Organization Installation grant (2151) and La Caixa Foundation (HR20-00361). This work was also partially supported by the ONEIDA project (LISBOA-01-0145-FEDER-016417) co-funded by Fundos Europeus Estruturais e de Investimento (FEEI) from 'Programa Operacional Regional Lisboa 2020' and by national funds from Fundação para a Ciência e a Tecnologia (FCT). S.R.J. was supported by NIH (R35 NS111631). Researchers were funded by individual fellowships from FCT (PD/BD/105838/2014 to I.J.V., 2020.06827.BD to L.S., SFRH/BD/80718/2011 to F.A.-B., PD/BD/138891/2018 to A.T. and CEECIND/03322/2018 to L.M.F.); a Novartis Foundation for Biomedical-Biological research to J.P.d.M.; a Human Frontier Science Programme long-term postdoctoral fellowship to M.D.N. (LT000047/2019); a Marie Skłodowska-Curie Individual Standard European Fellowship to S.S.P. (grant no. 839960); the GlycoPar Marie Curie Initial Training Network (GA 608295) to J.A.R. We thank J. Thomas-Oates (University of York, Centre of Excellence in Mass Spectrometry, Department of Chemistry) for the mass spectrometry analysis. The York Centre of Excellence in Mass Spectrometry was created thanks to a major capital investment through Science City York, supported by Yorkshire Forward with funds from the Northern Way Initiative, and subsequent support from EPSRC (EP/K039660/1 and EP/M028127/1). We also thank A. Temudo, A. Nascimento and A. Lima for bioimaging assistance; the laboratories of A. Tomás and J. Kelly for providing RNA from *Leishmania* and *T. cruzi*, respectively; and A. Pena and members of the Figueiredo and Jaffrey laboratories for helpful discussions.

Author contributions I.J.V., J.P.d.M., L.S., M.D.N., A.T., S.S.P., A.H.M., E.B. and J.A.R. performed the experiments. I.J.V., J.P.d.M., L.S., M.D.N., A.T., S.S.P., A.H.M., E.B., J.A.R., F.A.-B., S.R.J. and L.M.F. planned the experiments and analysed the data. I.J.V., F.A.-B., J.A.R., S.R.J. and L.M.F. conceived the study. I.J.V., S.R.J. and L.M.F. wrote the manuscript, with contributions of all remaining authors.

Competing interests The authors declare no competing interests.

Additional information
Supplementary information The online version contains supplementary material available at https://doi.org/10.1038/s41586-022-04544-0.
Correspondence and requests for materials should be addressed to Luisa M. Figueiredo.
Peer review information *Nature* thanks David Horn and the other, anonymous, reviewer(s) for their contribution to the peer review of this work. Peer reviewer reports are available.

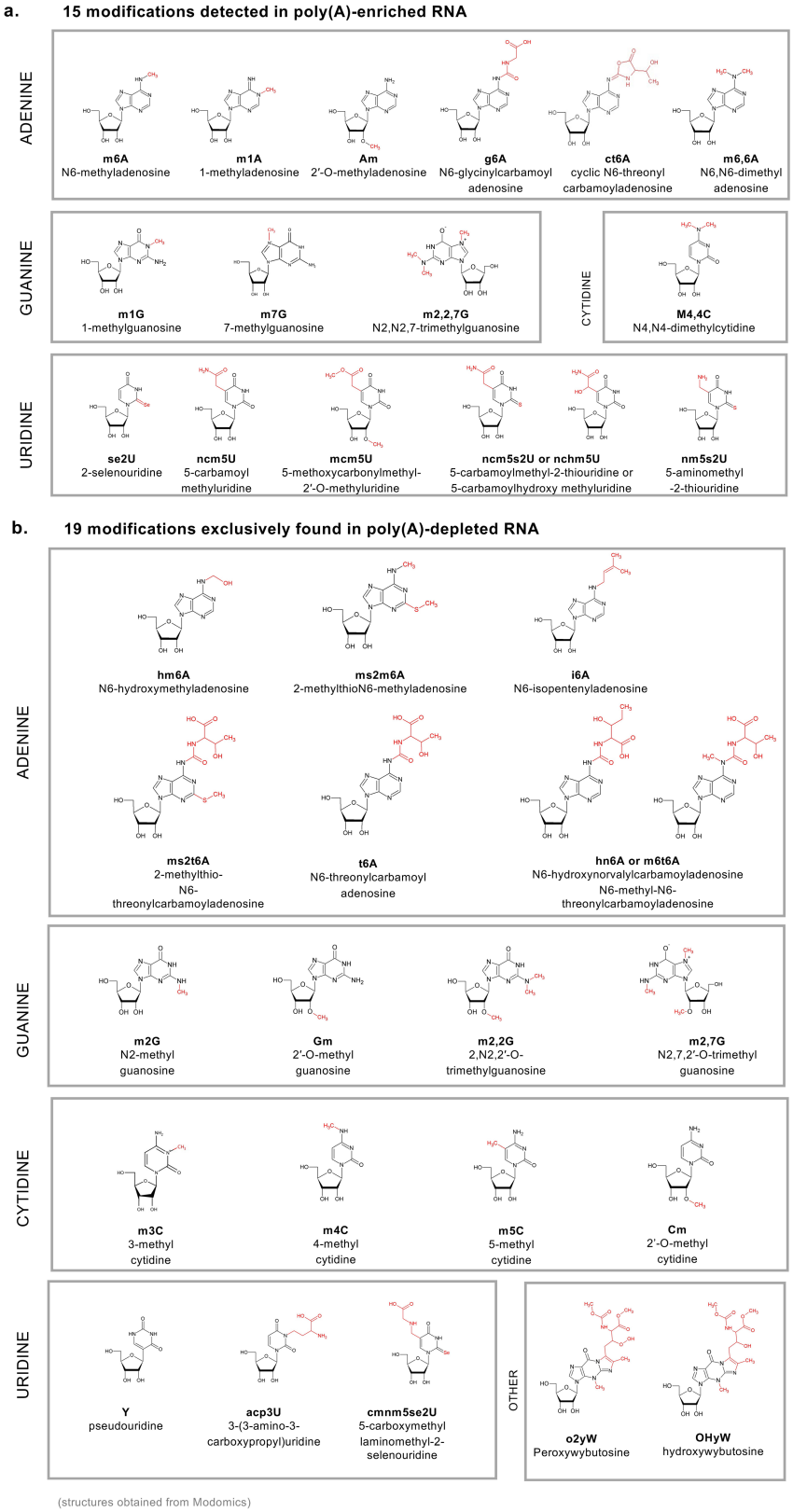

Extended Data Fig. 1 | Chemical structures of RNA modifications found in *T. brucei*. **a**, 15 modifications were detected in poly(A)-enriched RNA (mRNA). **b**, 19 modifications were not detected in poly(A)-depleted RNA. All modifications were detected in total RNA. Structures were obtained from the database Modomics (http://genesilico.pl/modomics/).

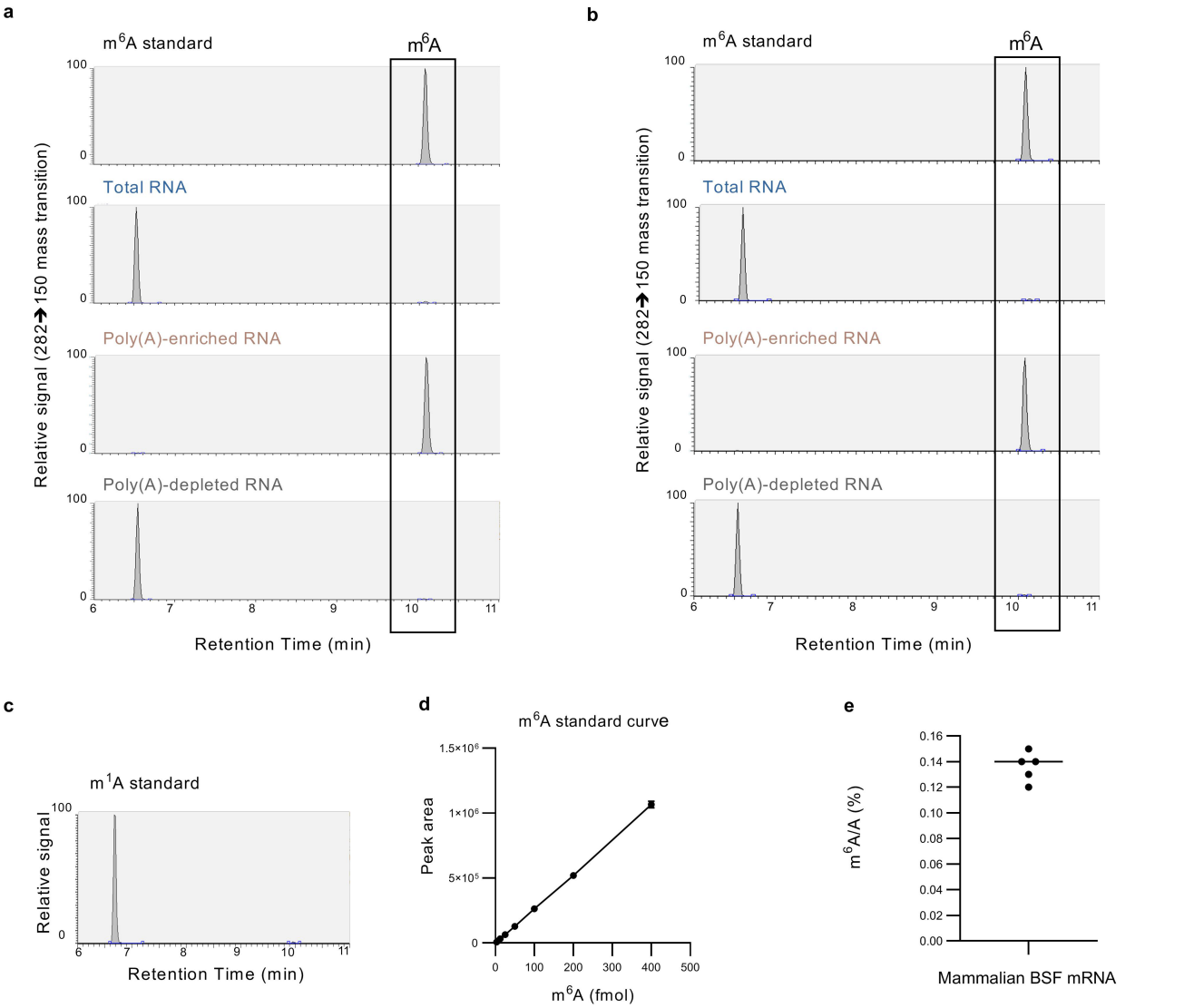

Extended Data Fig. 2 | Detection of m^{6}A in *T. brucei* by mass-spectrometry. **a**, **b**, Chromatograms obtained by LC-MS/MS analysis of a N6-methyladenosine standard and three RNA samples of *T. brucei* bloodstream form (BSF, **a**) or insect procyclic stage (PCF, **b**): total RNA, RNA enriched with poly(T)-beads (i.e., poly(A)-enriched RNA) and RNA that did not bind to polyT-beads (i.e., poly(A)-depleted RNA). **c**, Chromatogram obtained by LC-MS/MS analysis of a N1-methyladenosine standard with the 282->150 mass transition. The m^{1}A peak is detected at 6.5 min. **d**, Standard curve of m^{6}A. Increasing quantities of commercially synthesized m^{6}A were loaded on the HPLC column and the area under the chromatogram peak was measured. **e**, Quantification of the m^{6}A/A(%) in the mRNA in a second independent experiment. n = 5 mRNA samples. (see also Source Data of Extended Figures).

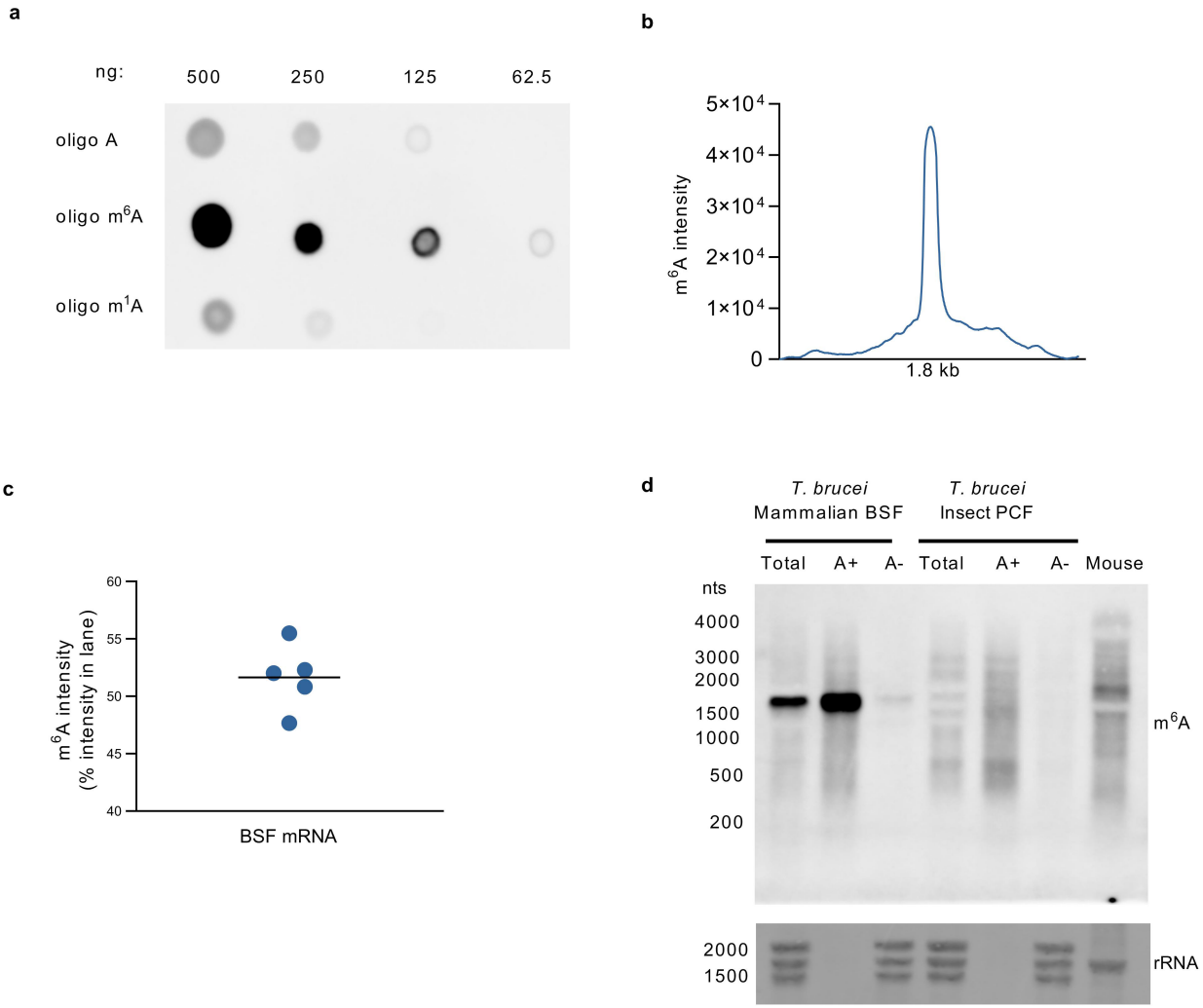

Extended Data Fig. 3 | m^{6}A detection in *T. brucei* by immunoblotting. **a**, Specificity of anti-m^{6}A antibody. Oligonucleotides containing either m^{6}A (positive control), unmodified adenosine or m^{1}A (negative controls) were manually spotted in the membrane, which was incubated with anti-m^{6}A antibody. The antibody specifically recognized the oligos with m^{6}A, while exhibiting low cross-reactivity to the oligos with only unmodified adenosine or containing m^{1}A. **b**, m^{6}A signal intensity in the immunoblot, measured by Image J, in the whole lane containing the poly(A)-enriched RNA of bloodstream forms. **c**, The intensity of the ~1.8 kb band was divided by the signal intensity of the entire lane. n = 5 biological replicates. **d**, m^{6}A immunoblotting of RNA samples from two stages of *T. brucei* life cycle. Samples (from left to right): total RNA (Total), Poly(A)-enriched (A+) RNA and Poly(A)-depleted (A-) RNA from mammalian BSF and insect PCF. The last lane contains total mouse liver RNA (Mouse). 2 µg of total RNA, 2 µg of poly(A)-depleted RNA and 100 ng of poly(A)-enriched RNA was loaded per lane. rRNA was detected by staining RNA with methylene blue to confirm equal loading between total and poly(A)-depleted fractions. As expected rRNA is undetectable in the poly(A)-enriched fraction. (see also Supplementary Fig. 1 and Source Data of Extended Figures).

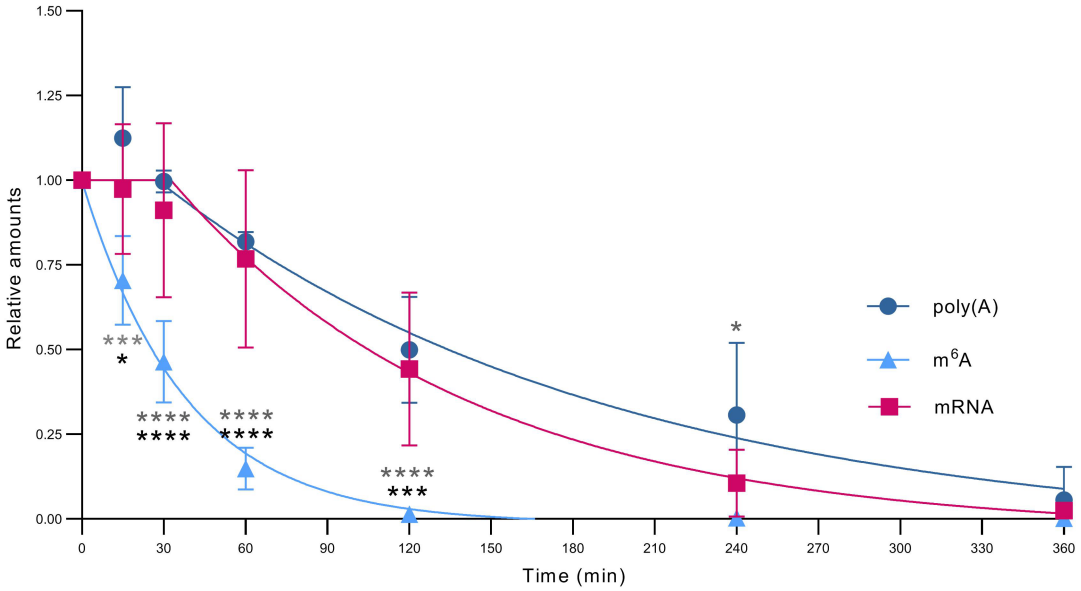

Extended Data Fig. 4 | Poly(A) tail length, m^{6}A and mRNA levels during VSG turnover. Levels of m^{6}A (immunoblot), length of VSG poly(A) tail (RNase H – northern blot) and levels of VSG mRNA (northern blot) after transcription halt by ActD. Signals were normalized to time point 0hr. The pattern observed is consistent with Fig. 2b. Two-way ANOVA with sidak correction for multiple test. (****$P < 0.0001$,*$P = 0.0190$ in mRNA vs m6A in 15 min, ***$P = 0.0004$ in poly(A) vs m6A in 15 min, ***$P = 0.0001$ in mRNA vs m6A in 120 min, *$P = 0.0136$ in poly(A) vs m6A in 240 min). n = 4 biological samples for mRNA and m^{6}A levels, n = 3 biological samples for poly(A) tail length. Data are mean ± s.d. (see also Source Data of Extended Figures).

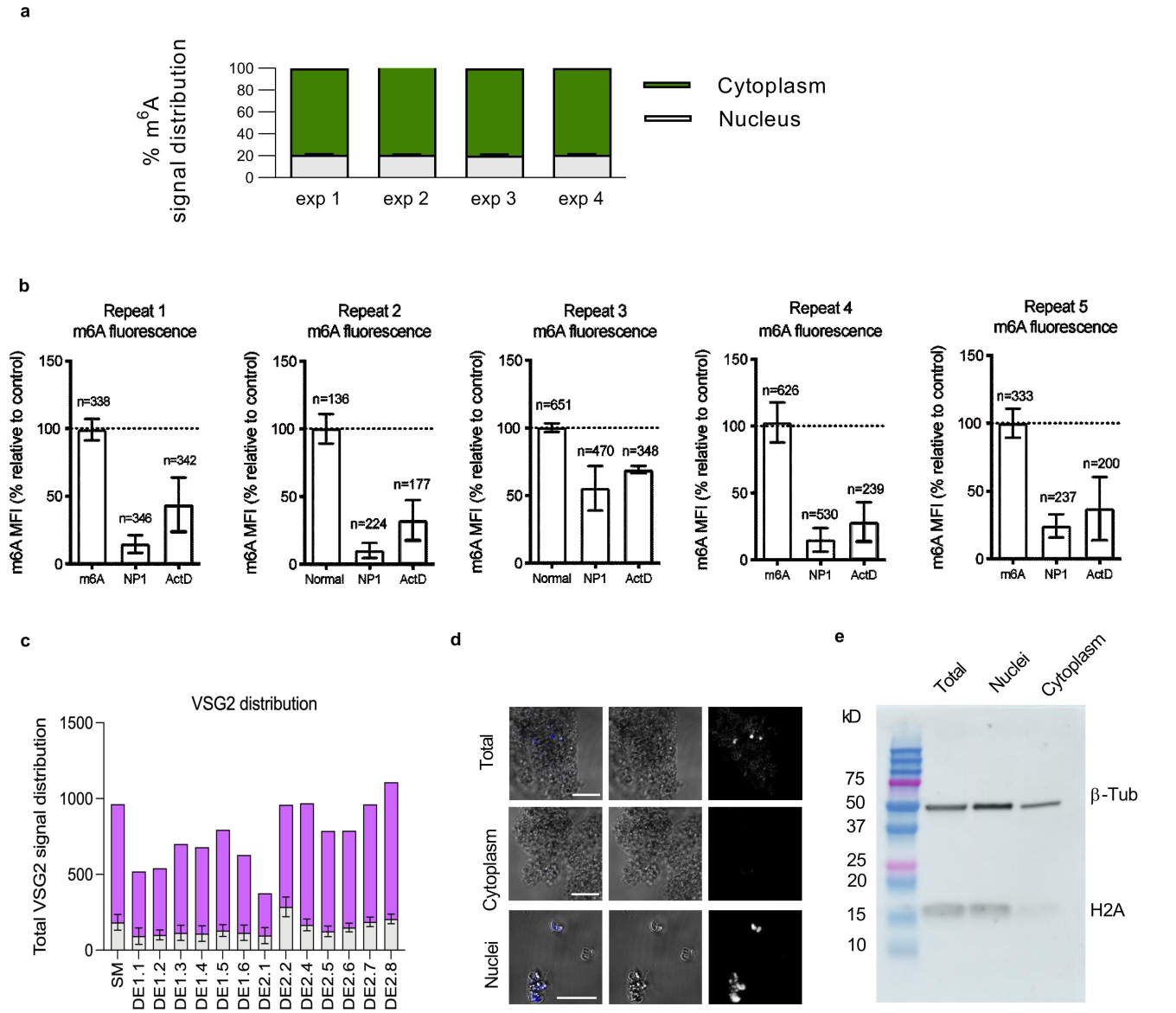

Extended Data Fig. 5 | Subcellular distribution of m^{6}A in bloodstream form parasites. a, Proportion of m^{6}A signal in nucleus and cytoplasm. Data are mean ± s.e.m. n = 4 independent experiments. **b**, Quantification of mean fluorescence intensity (MFI) levels of m^{6}A in five independent replicates in three different conditions: untreated BSF, nuclease P1 (NP1)-treated BSF, and actinomycin D (ActD)-treated BSF. Raw MFIs were obtained, the average of the untreated BSF equalled to 100%, and all other values normalized to 100%. Data are mean ± s.e.m. **c**, Distribution of VSG2 mRNA in the nucleus and cytoplasm in single marker (SM) cell line (single VSG expression) and in the clones that express a second reporter VSG (6 clones of DE1 express VSG117 containing a WT 16-mer motif, 7 clones of DE2 express VSG117 containing a mutagenized 16-mer motif). VSG mRNA was quantified by FISH. Nucleus was delimited by Hoechst staining. Total signal was set as 100% and the nucleus and cytoplasm represented as percentage of total signal. Error bars represent s.d. **d**, Microscopic observation of nuclei purified after fractionation protocol. Nuclei were stained with Hoechst. The nuclear purification was compared with initial lysates and with the cytoplasmic fraction. Scale bars, 10 µm; $n = 1$ independent experiment. **e**, Western blot of subcellular fractions (total lysate, nuclear and cytoplasmic fractions) using antibodies against a nuclear protein (histone H2A; custom rabbit polyclonal 1:5000) and a cytoplasmic protein (β-tubulin; mouse monoclonal KMX-1 1:1000). For each sample, we loaded a protein equivalent to the same amount of cells. n = 3 independent experiments. (see also Supplementary Fig. 1 and Source Data of Extended Figures).

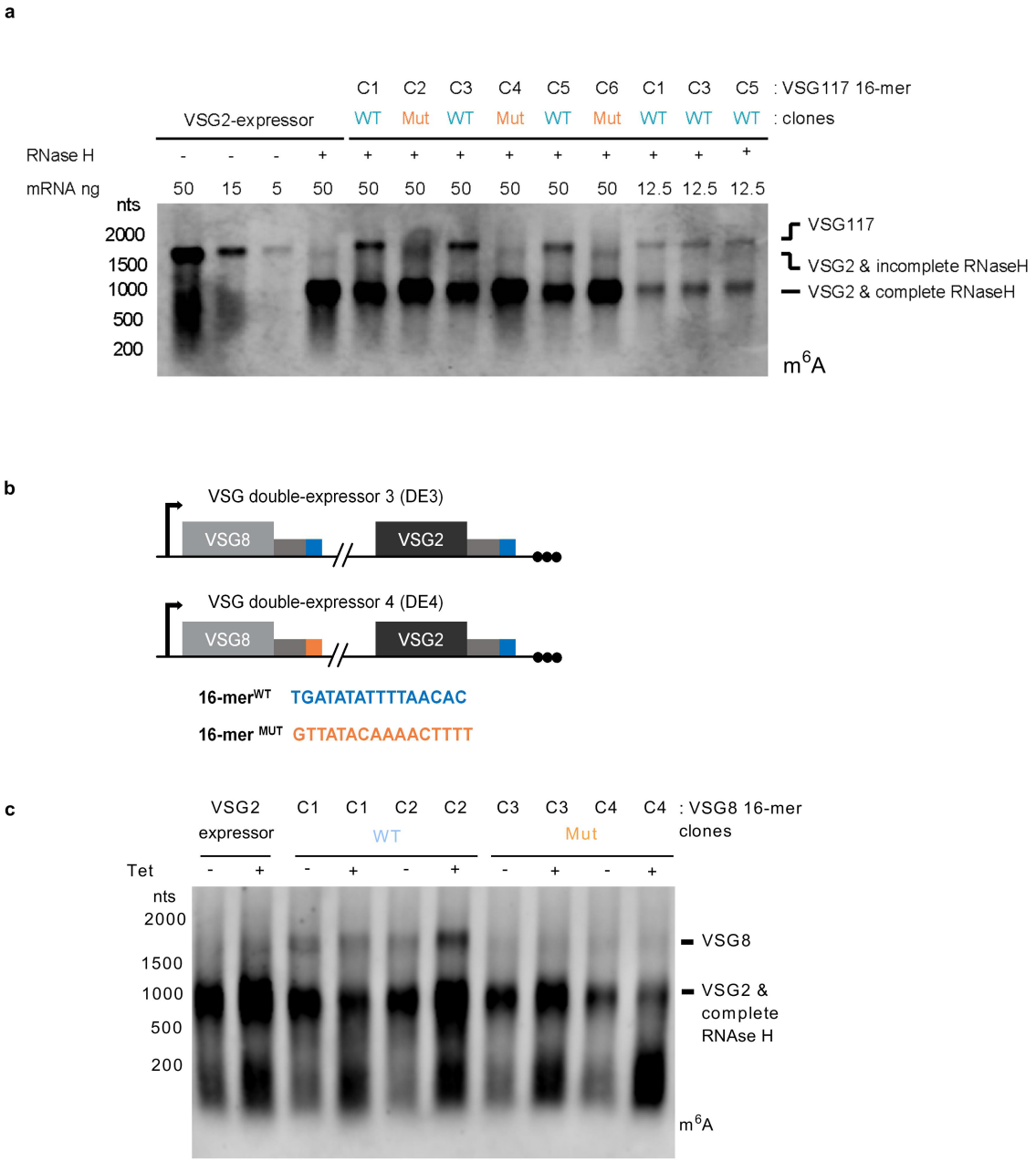

Extended Data Fig. 6 | VSG double-expressor (DE) cell lines immunoblotting. a, Overexposure of full immunoblot shown in Fig. 4c. Three independent 16-mer^{WT} clones and three independent 16-mer^{MUT} are shown (C1–C6). Note that with this exposure, most intense bands are saturated. The purpose of this high exposure is to observe the region of blot corresponding to the VSG117 transcript. No VSG117 band is observed in the 16-mer^{MUT} clones. It is also possible to observe a weak VSG2 band in the VSG2 single expressor lane and in the 16-mer^{MUT} clones, which correspond to incomplete RNase H digestion of VSG2 transcript. $n = 3$ independent clones for each genotype (C1–C6). **b**, Schematics of VSG double-expressor (DE) cell-lines DE3 and DE4. *VSG8* was inserted in the active bloodstream expression site, which naturally contains *VSG2* at the telomeric end. In DE3, *VSG8* contains its endogenous 3'UTR with the conserved 16-mer motif (sequence in blue). In DE4, the 16-mer motif of *VSG8* was scrambled (sequence in orange). **c**, m^{6}A immunoblot of mRNA from DE3 and DE4 cell-lines, in which CAF1 was further depleted by RNAi by adding Tetracycline (Tet). RNase H digestion of *VSG2* mRNA was used to resolve *VSG2* and *VSG8* transcripts. Two independent DE3 clones and two independent DE4 clones are shown (C1–C4), each with (+) or without (−) CAF1 downregulation. (see also Supplementary Fig. 1).

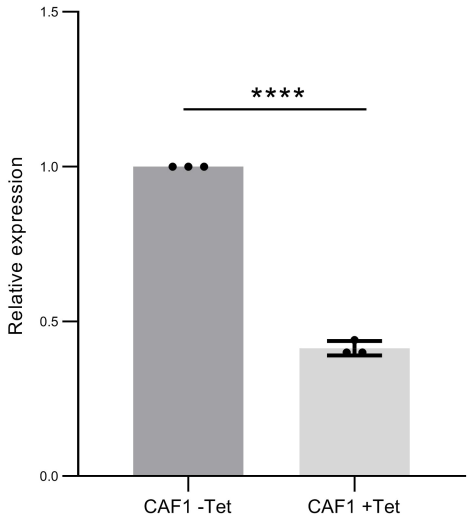

Extended Data Fig. 7 | CAF1 depletion. CAF1 transcript levels measured by RT-qPCR in CAF1 RNAi cell-line used in Fig. 5c–f. CAF1 downregulation was induced by adding tetracycline (Tet) to the medium. Unpaired two tailed t-test (**** $P > 0.0001$). Data are mean ± s.d. n = 3 independent clones.

Extended Data Table 1 | Mass-spectrometry features of 34 nucleoside modifications found in *T. brucei*

Base	Modification	Mass transition	Retention time (min)
Adenosine	m^6A	282>150	9.90
	m^1A	282>150	6.66
	Am	282>136	9.38
	g^6A	369>237	8.47
	ct^6A	395>263	6.90
	$m^{6,6}A$	296>164	11.80
	hm^6A	298>166	9.93
	ms^2m^6A	328>196	6.0
	i^6A	336>204	16.63
	ms^2t^6A	459>327	13.94
	t^6A	413>281	12.76
	hn^6A or m^6t^6A	427>295	13.89
Guanosine	m^1G	298>166	8.46
	m^7G	298>166	7.45
	$m^{2,2,7}G$	328>196	5.36
	m^2G	298>166	9.58
	Gm	298>152	9.80
	$m^{2,2}G$	312>180	10.70
	$m^{2,7}G$	312>180	8.58
Cytidine	$m^{4,4}C$	272>140	7.94
	m^3C	258>126	6.42
	m^4C	258>126	7.96
	m^5C	258>126	6.76
	Cm	258>112	7.81
Uridine	se^2U	306>174	8.45
	ncm^5U	302>170	7.96
	mcm^5U	317>185	7.95
	ncm^5s^2U or $nchm^5U$	318>186	8.47
	nm^5s^2U	290>158	5.36
	Y	245>125	4.5
	acp^3U	346>214	6.55
	$cmnm^5se^2U$	394>262	8.47
Other	OHyW	525>393	5.37
	o^2yW	541>409	5.39

Extended Data Table 2 | List of oligonucleotides

PURPOSE	SEQUENCE
AnTaT VSG qPCR	ACAACCACGGAAAGTGACG
	CACTTTTTGTCGCCATAAGC
VSG2 qPCR	AGCAGCCAAGAGGTAACAGC
	CAACTGCAGCTTGCAAGGAA
VSG117 qPCR	AAGCGACAACAGATAAATGC
	CTTTGCAAGCATTATTTTCC
18S qPCR	ACGGAATGGCACCACAAGAC
	GTCCGTTGACGGAATCAACC
16-mer mutagenesis	TTTGTTATACAAAACTTTTCAAAACCAGCCGAGATTTTGTG
	TTTGAAAAGTTTTGTATAACAAAAGTTTTCAAGTAGCAAGG
PAT adaptor	5'-Ph-CCAGTGAGCAGAGTGACGAGGACTCGAGCTCAAGC-3ddA-3'
PAT Rev_1	GCTTGAGCTCGAGTCCTCG
PAT Rev_2	CGTCACTCTGCTCACTGG
PAT rev A0	GAGGACTCGAGCTCAAGCGCGTGTTAAAATATATCAG
PAT AnTaT 1	AATCCCCGAATTGTAAATGG
PAT AnTaT 2	TTTCTGCCGCATTTGTGG
PAT VSG117 1	AAGCGACAACAGATAAATGC
PAT VSG117 2	ATTCGCCCTCAGTGCTGC
AnTaT VSG RNase H A	TACTCGTCGTTGGCTGCTTG
AnTaT VSG RNase H B	TATTTTACTGCATAGGGCGT
AnTaT VSG RNase H C	GCGTGTTAAAATATATCAGA
Spliced leader RNase H	CAATATAGTACAGAAACTGT
β-tubulin RNase H	TACGGAGTCCATTGTACCTG
Oligo d(T)	TTTTTTTTTTTTTTTTT
VSG2 RNase H	TCCGGCTGTTTCGTTTCT
Dot blot oligo A	ACTAGCTTAACTACGACCTCCTGAG
Dot blot oligo m^6A	ACTAGCTTAACT-m^6A-CGACCTCCTGAG
Dot blot oligo m^1A	ACTAGCTTAACT-m^1A-CGACCTCCTGAG
VSG8 cloning	GGAGAAAGAATAGTAACCCTTTCATCAAAGAAAATAGTCGAA
	GCTTATGCGAACAGCGAGCACAACC
	GAGGGGGGAAATTTGAGGGGGGAAAGGGCTGCAGGAATTC
	TTAAAAAAGCAAGGCCACAAATGC
VSG8 qPCR	ATGGAAAGGAACCAACAACG
	CCCTCCTTTGTCTTATCTTTGC
CAF1 qPCR	GGAGTTTGGTATAATCCGTTCG
	GCGTGGATTTGAAGTTACCG
PAT VSG2 1	AAGGTAGCAGATGAGACTGC
PAT VSG2 2	TTAGCAAGACCCCTCTTTGG
VSG RNase H northern	ACGCCCTATGCAGTAAAATA
VSG motif probe	GCGTGTTAAAATATATC

Extended Data Table 3 | Statistical parameters of time course experiments

Figure	Measure	Experimental approach	Curve fit	Lag phase (X0) (min)	Decay constant (K) (min^{-1})	Half-life (min)	R^2
2b	mRNA	Transcription inhibition (ActD)	Biphasic	60.0	0.019	36.9	0.91
2b	poly(A)	Transcription inhibition (ActD)	Biphasic	42.9	0.015	45.4	0.95
2b	m^6A	Transcription inhibition (ActD)	Exponential	NA	0.019	37.4	0.93
2d	mRNA	Differentiation	Biphasic	53.5	0.012	58.7	0.88
2d	poly(A)	Differentiation	Exponential	NA	0.031	22.7	0.93
5d	mRNA	Transcription inhibition (ActD)	Exponential	NA	0.019	36.8	0.95
5b	poly(A)	Transcription inhibition (ActD)	Exponential	NA	0.074	9.3	0.98
S4	mRNA	Transcription inhibition (ActD)	Biphasic	32.7	0.009	76.3	0.85
S4	poly(A)	Transcription inhibition (ActD)	Biphasic	27.8	0.006	114.5	0.91
S4	m^6A	Transcription inhibition (ActD)	Exponential	NA	0.026	26.2	0.97

Curves were fitted to the decay of *VSG* mRNA (pink), length of poly(A)-tail (dark blue) and m^6A levels (light blue). Curves in which the measured variable decayed from T=0 h were called "One phase". Those in which the measured variable decayed only after an initial constant period were called "Biphasic".

nature research

Corresponding author(s): Figueiredo L.M

Last updated by author(s): Jan 13, 2022

Reporting Summary

Nature Research wishes to improve the reproducibility of the work that we publish. This form provides structure for consistency and transparency in reporting. For further information on Nature Research policies, see Authors & Referees and the Editorial Policy Checklist.

Statistics

For all statistical analyses, confirm that the following items are present in the figure legend, table legend, main text, or Methods section.

n/a	Confirmed
☐	☒ The exact sample size (*n*) for each experimental group/condition, given as a discrete number and unit of measurement
☐	☒ A statement on whether measurements were taken from distinct samples or whether the same sample was measured repeatedly
☐	☒ The statistical test(s) used AND whether they are one- or two-sided *Only common tests should be described solely by name; describe more complex techniques in the Methods section.*
☐	☒ A description of all covariates tested
☐	☒ A description of any assumptions or corrections, such as tests of normality and adjustment for multiple comparisons
☐	☒ A full description of the statistical parameters including central tendency (e.g. means) or other basic estimates (e.g. regression coefficient) AND variation (e.g. standard deviation) or associated estimates of uncertainty (e.g. confidence intervals)
☐	☒ For null hypothesis testing, the test statistic (e.g. *F*, *t*, *r*) with confidence intervals, effect sizes, degrees of freedom and *P* value noted *Give P values as exact values whenever suitable.*
☒	☐ For Bayesian analysis, information on the choice of priors and Markov chain Monte Carlo settings
☒	☐ For hierarchical and complex designs, identification of the appropriate level for tests and full reporting of outcomes
☒	☐ Estimates of effect sizes (e.g. Cohen's *d*, Pearson's *r*), indicating how they were calculated

Our web collection on statistics for biologists contains articles on many of the points above.

Software and code

Policy information about availability of computer code

Data collection	Amersham ImageQuant 800 Cytiva 2.0.0, Thermo Scientific TM XcaliburTM software
Data analysis	Thermo Scientific TM XcaliburTM software, STAR, SAMtools, stringtie, EdgeR, limma-voom packages, Fiji/ImageJ, Imaris 9.1.0 , GraphPad Prism Software versions 5-8

For manuscripts utilizing custom algorithms or software that are central to the research but not yet described in published literature, software must be made available to editors/reviewers. We strongly encourage code deposition in a community repository (e.g. GitHub). See the Nature Research guidelines for submitting code & software for further information.

Data

Policy information about availability of data

All manuscripts must include a data availability statement. This statement should provide the following information, where applicable:

- Accession codes, unique identifiers, or web links for publicly available datasets
- A list of figures that have associated raw data
- A description of any restrictions on data availability

- Datasets of RNA-seq of m6A-RIP experiments (three input samples and three precipitated samples) are deposited in SRA accession code: PRJNA786734
- Figures with associated raw: 1b, 1c, 1e, 1h, 2b, 2c, 3c, 3d, 3f, 3g, 3i, 3k, 4b, 4e, 4f, 5b, 5c, 5d, 5f, ext2d, ext2e, ext3c, ext4, ext5a, ext5b, ext5c, ext7
- Publically available Trypanosome genome database (TryTrypDB): https://tritrypdb.org/tritrypdb/app
-Publically available RNA modifications database (MODOMICS): http://genesilico.pl/modomics/
- All data is available upon request.

Field-specific reporting

Please select the one below that is the best fit for your research. If you are not sure, read the appropriate sections before making your selection.

☒ Life sciences ☐ Behavioural & social sciences ☐ Ecological, evolutionary & environmental sciences

For a reference copy of the document with all sections, see nature.com/documents/nr-reporting-summary-flat.pdf

Life sciences study design

All studies must disclose on these points even when the disclosure is negative.

Sample size	Most experiments were performed with 3 independent replicates. This number was selected based on two criteria. Most differences found between sample groups were very large (eg. Figures 1B) or the data consists of a time-series in which the overall trend was used to compare groups (eg. Figure 3B).
Data exclusions	One poly(A) enriched insect PCF sample was discarded due to abundant ribosomal RNA contamination (figure 1 b).
Replication	The findings were reproduced within our lab or Samie Jaffrey's lab. Some of the experiments (RT-qPCR, RNase H digestion, m6A immunoblot) were performed independently by two different investigators (Idalio Viegas and Juan Pereira de Macedo or Lucia Serra). Figure 1H, the replication was limited by the acessibility to RNA samples from other species of trypanosomatids, that were not being cultivated in the lab. The samples used were kindely provided from other investigators. Human RNA was one replicate becouse was used as tecnical control of the method.
Randomization	The random allocation is not relevant to our study because we mostly use identical culture conditions and thus no confounding factors are expected to be found between groups. All experiments were performed on parasites cultured in identical flasks, in the same incubators, with the same media, in the same tissue culture room.
Blinding	Researchers were not blinded to the group allocation because we did not envision how a possible biased behaviour could affect the interpretation of the results. Besides, in experiments where CAF1 knock-down was induced by tetracyclin, the researcher had to know to which flask tetracyclin should be added. Finally, in some instances, a second variable (not at test) revealed the identity of the samples. However, in some experiments two researchers obtained identical results.

Reporting for specific materials, systems and methods

We require information from authors about some types of materials, experimental systems and methods used in many studies. Here, indicate whether each material, system or method listed is relevant to your study. If you are not sure if a list item applies to your research, read the appropriate section before selecting a response.

Materials & experimental systems

n/a	Involved in the study
☐	☒ Antibodies
☐	☒ Eukaryotic cell lines
☒	☐ Palaeontology
☒	☐ Animals and other organisms
☒	☐ Human research participants
☒	☐ Clinical data

Methods

n/a	Involved in the study
☒	☐ ChIP-seq
☒	☐ Flow cytometry
☒	☐ MRI-based neuroimaging

Antibodies

Antibodies used	Rabbit anti-m6A polyclonal antibody (Abcam ab151230); HRP-conjugated donkey anti-rabbit IgG (GE Healthcare, NA934); HRP-conjugated sheep anti-mouse IgG (GE Healthcare, NXA931); Alexa Fluor 488 conjugated goat anti-rabbit (Thermo Fisher Scientific-lifetecnologies A11034); Anti-Histone H2A: custom-made rabbit antibody. KMX-1 is monoclonal antibody against b-tubulin from Keith Gull's laboratory. (https://febs.onlinelibrary.wiley.com/doi/abs/10.1016/0014-5793(85)81244-8)
Validation	The manufacturer provides the antibody with the following description: "All batches of ab151230 are tested in Nucleotide Array against N6-methyladenosine (m6A) and unmodified adenosine". Additionally, our results indicate the suitability of the antibody

for m6A detection by dot blot against DNA oligos containing methylated adenosines, m6A (positive control) or m1A, or without any modification (negative control) (Figure S2).

Anti-Histone H2A is a custom-made rabbit antibody and it was validated in PMID: 26673706. KMX-1 is a custom-made monoclonal antibody from Keith Gull's laboratory and it was validated in PMID: 4018260.
Alexa Fluor 488 conjugated goat anti-rabbit (Thermo Fisher Scientific-lifetecnologies A11034) is tested by the manufacturer for several experimental methods, including IFA. Additionally, we did econdary only controls (absence of primary antibody) to check absence of signal.

Eukaryotic cell lines

Policy information about cell lines

Cell line source(s)	EATRO 1125 AnTat1.1 90:13 from Keith Matthews laboratory (The University of Edinburgh, UK) and Lister 427 antigenic type MiTat 1.2, clone 221a, Single Marker (SM) from George Cross laboratory (The Rockefeller University, New York, USA). HEK293T cell-line was commercially purchased.
Authentication	The cell-lines were not authenticated.
Mycoplasma contamination	The cell-lines were not tested for Mycoplasma contamination.
Commonly misidentified lines (See ICLAC register)	None of the cell lines are listed in ICLAC.